

**DESIGN OF A SINGLE SIDED LINEAR INDUCTION MOTOR
(SLIM) USING A USER INTERACTIVE COMPUTER PROGRAM**

A Thesis presented to the faculty of the Graduate School
University of Missouri-Columbia

In Partial Fulfillment
Of the Requirements for the Degree
Master of Science

by
SARVESWARA PRASAD BHAMIDI

Dr. Robert M O'Connell, Thesis Supervisor

May 2005

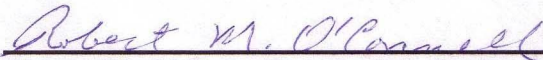
The undersigned appointed by the Dean of the Graduate School, have examined the thesis entitled

DESIGN OF SINGLE SIDED LINEAR INDUCTION MOTOR (SLIM)
USING A USER-INTERACTIVE COMPUTER PROGRAM

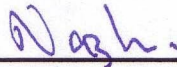
presented by Sarveswara Prasad Bhamidi

a candidate for the degree of Master of Science

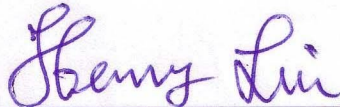
and hereby certify that in their opinion is worthy of acceptance.



Robert M. O'Connell, Associate Professor, Department of Electrical Engineering



Naz Islam, Associate Professor, Department of Electrical Engineering



Henry Liu, Professor Emeritus, Department of Civil Engineering

Dedicated to my parents

Bhagya Lakshmi and Venkata Ramana Rao

ACKNOWLEDGEMENTS

MatrudEvObhava”, “PitrudEvobhava”, ‘AchAryadEvOBHava” AthidhidEvOBHava”. These are four MahAvAkyAs from the Upanishads which means pray your mother, pray your father, pray your guru, and pray your guest.

With these words of wisdom, I want to start the endless list of my family members, friends, and teachers who supported throughout my life. The first word I learnt is “Amma” which means mother. I remember the first step that I took with the help of my father. I sincerely want to thank my mother Bhagya Lakshmi and my father Ramana Rao without whom my dream wouldn’t have come true. I’m very grateful to my sister, Kumari, my brother-in-law, Sastry, my brother, Sridhar and my cute little niece, Aditi, whose endless cheering and encouragement made this world a beautiful place to live in.

The best part of my studies at University of Missouri is to have Dr. Robert O’Connell as my advisor. Without his relentless efforts, timely guidance and constant support, this project wouldn’t have been successful. I sincerely thank him for his encouragement and kind nature throughout this project.

I also want to thank Dr. Henry Liu who is one of the world’s renowned experts in capsule pipeline technology and Dr. Lenau Charles who helped me a lot in understanding the practical point of view of this project and its importance in real world. Their

experience and expertise in the field of pneumatic capsule pipeline transport systems helped me to learn a lot. I also want to appreciate and thank Dr. Naz Islam who readily accepted my invitation to be a member of my Thesis committee. I also want to extend my sincere acknowledgements to Kelly and Betty of Electrical Engineering Department who helped me a lot during my stay at MU.

I'm very grateful to my group of friends "Elegant Electricals 4 Ever", in India and abroad, who stood by my side and encouraged me a lot all throughout my career. Special thanks to my close buddies Bujji, Deeps, Vassu, Sakki, Thati, Kallu and Chandan whose constant support and encouragement made my stay in USA a pleasant and memorable one. I also want to thank my room mates Chaitu, Kranthi and Rahul for their caring, affection and support which helped me a lot to become a better person. I convey my special thanks and gratitude to a wonderful person, Dharani, my friends Suman, Sagar Uday and Pramod who boosted my courage and supported me all the way.

I dedicate my life, my work, and whatever I have achieved in my life so far to my parents.

TABLE OF CONTENTS

ACKNOWLEDGEMENTS	ii
LIST OF ILLUSTRATIONS.....	vii
LIST OF TABLES.....	ix
LIST OF SYMBOLS	x
ABSTRACT	xv
CHAPTER	
1. INTRODUCTION.....	1
2. LITERATURE REVIEW.....	5
3. SLIM THEORY AND EQUATIONS.....	12
3.1. SLIM Concept and Equations.....	13
3.1.1. The Concept of Current Sheet.....	15
3.1.2. Power Rating and Rated Input Phase Current.....	17
3.1.3. Flux Linkage and Induced Voltage.....	18
3.1.4. Equations for SLIM Slot Geometry.....	19

3.2.	Forces in LIM.....	21
3.2.1.	Thrust.....	22
3.2.2.	Normal Forces.....	22
3.2.3.	Lateral Forces.....	23
3.3.	SLIM Performance from Equivalent Circuit Model.....	23
3.3.1.	Equivalent Circuit Models and Components.....	24
3.4.	Thrust and Efficiency.....	27
3.5.	Edge Effects due to Secondary Overhangs.....	29
4.	DESIGN OF SLIM USING USER-INTERACTIVE PROCEDURE.....	34
4.1.	Winding Configurations of a SLIM.....	34
4.1.1.	Single Layer Windings.....	34
4.1.2.	Double Layer Windings.....	36
4.2.	SLIM Stator Unit Design.....	39
4.3.	Amounts of Materials Required for the Construction of One SLIM Stator Unit.....	51
5.	PERFORMANCE CURVES AND DISCUSSION OF RESULTS.....	64
5.1.	Characteristic Curves of SLIM.....	64
5.2.	Evaluation of Performance of SLIM by Changing Parameters....	68
5.2.1.	Effect of Aluminum thickness on the performance parameters.....	68
5.2.2.	Effect of Mechanical air-gap on performance.....	71
5.2.3.	Effect of changing number of poles on Performance.....	73
5.3.	Comparing the results of the SLIM and the TLIM of the same desired values.....	75

6. CONCLUSIONS AND SUGGESTIONS	77
6.1. Conclusions.....	77
6.2. Suggestions for future study.....	79
APPENDIX	
A. AWG Table for Copper Wire.....	80
B. A User-Interactive MATLAB program code for the design of SLIM.....	81
REFERENCES.....	88

LIST OF ILLUSTRATIONS

Figure	page
3.1. Imaginary Process of Unrolling a Conventional Motor to Obtain a LIM.....	13
3.2. Radius of a Rotary Induction Motor and Length of a SLIM.....	14
3.3. SLIM Geometry.....	19
3.4. Forces in a LIM.....	22
3.5. Per-Phase SLIM Equivalent Circuit.....	25
4.1. Single layer winding configuration for a 4 pole, 3 phase, 1 slot per pole per phase, SLIM.....	35
4.2. Flux distribution and back-iron density of a single layer winding.....	35
4.3. Fractional-pitch, Double layer winding for a 4 pole, 3 phase, 1 slot per pole per phase SLIM whose coil span is one-third the pole pitch.....	37
4.4. Fractional pitch, Double layer winding for a 4 pole, 3 phase, 1 slot per pole per phase SLIM whose coil span is two-thirds the pole pitch.....	37
4.5. Full-pitch, double layer winding for a 4 pole, 3 phase, 1 slot per pole per phase SLIM.....	38
4.6. Flow chart of the SLIM design procedure.....	41, 42
5.1. Thrust F_s versus rotor velocity V_r of one SLIM stator unit at a rated slip of 5%, a desired rotor velocity of 15.5 m/s, a target thrust of 8611N and final thrust of 9658N.....	66
5.2. Fig 5.2 Efficiency η versus rotor velocity V_r of one SLIM stator unit at a rated slip of 5%, a desired rotor velocity of 15.5 m/s and target thrust of 8611N.....	66
5.3. Thrust F_s versus rotor velocity V_r of one SLIM stator unit at a rated slip of 10%, a desired rotor velocity of 15.5 m/s, a target thrust of 8611N and a final thrust of 8610N.....	67

5.4.	Efficiency η versus rotor velocity V_r of one SLIM stator unit at a rated slip of 10%, a desired rotor velocity of 15.5 m/s and target thrust of 8611N.....	67
5.5.	Effect of aluminum thickness on the thrust of SLIM plotted against rotor velocity for the design 2 in table 4-8.....	70
5.6.	Effect of varying Aluminum thickness on efficiency of SLIM plotted against rotor velocity for the design 2 in table 4-8.....	70
5.7.	Effect of mechanical air-gap on thrust of SLIM at a rated slip of 10% and a target thrust of 8611 N for the design 2 in table 4-8.....	72
5.8.	Effect of mechanical air-gap on efficiency of SLIM at a rated slip of 10% and a target thrust of 8611 N for the design 2 in table 4-8.....	73
5.9.	Effect of changing poles on the thrust developed by a SLIM versus rated rotor velocity for the design 2 in table 4-8.....	74
5.10.	Effect of changing poles on the efficiency of a SLIM plotted against rated rotor velocity for the design 2 in table 4-8.....	75

LIST OF TABLES

Table	Page
4-1. Necessary Constants in the design of SLIM.....	40
4-2. Desired values of some of the parameters of SLIM.....	43
4-3. Variation of actual thrust with number of turns per slot.....	53
4-4. Design parameters of SLIM at 10% slip and target thrust of 8611N.....	55
4-5. Design parameters of SLIM at 10% slip and target thrust of 8171N.....	56
4-6. Design parameters of SLIM at 5% slip and target thrust of 8611N.....	57
4-7. Design parameters of SLIM at 5% slip and target thrust of 8171N.....	58
4-8. Improved design parameters of SLIM at 10% slip and target thrust of 8611N.....	60
4-9. Improved design parameters of SLIM at 10% slip and target thrust of 8171N.....	61
5-1. Aluminum sheet thickness effects on thrust and efficiency at rated rotor velocity.....	69
5-2. Air-gap effects on thrust and efficiency.....	71
5-3. Effect of changing number of poles on the performance.....	74
5-4. Comparison of the TLIM and the SLIM of same desired values.....	76

LIST OF SYMBOLS

Symbol	Physical Quantity	SI Unit
A_s	Area of slot	Square meter, m ²
A_w	Area of copper wire for one turn per slot	Square meter, m ²
A_{wt}	Total area of copper wire	Square meter, m ²
B_{gavg}	Average air-gap magnetic flux density	Tesla (Wb/m ²), T
B_{gmax}	Maximum air-gap magnetic flux density	Tesla (Wb/m ²), T
B_{imax}	Maximum tooth flux density	Tesla (Wb/m ²), T
B_{ymax}	Maximum yoke flux density	Tesla (Wb/m ²), T
d	Thickness of aluminum sheet on Rotor	Meters, m
D_w	Diameter of Copper wire	Meters, m
e	Induced voltage per turn in a coil	Volts, V
E_l	RMS Induced Voltage in a coil	Volts, V
f	frequency	Hertz, Hz
F_s	Electromagnetic thrust generated by rotor	Newtons (Kg.m/s ²), N
F_s'	Estimated Electromagnetic thrust generated by rotor	Newtons(Kg.m/s ²), N
F_n	Normal Force	Newtons (Kg.m/s ²), N
g_e	Equivalent air-gap	Meters, m
g_{ei}	Equivalent air-gap considering edge effects	Meters, m

g_m	Mechanical air-gap	Meters, m
g_0	Magnetic air-gap	Meters, m
G	Goodness factor	-
G_{ei}	Equivalent Goodness Factor	-
h_s	Slot height	Meters, m
h_y	Yoke Height	Meters, m
I_1	RMS Input Phase Current	Amperes, A
I_1'	Estimated RMS Input Current	Amperes, A
I_2	Rotor Phase Current	Amperes, A
I_m	Magnetizing current	Amperes, A
J_1	Stator Current Density	Amperes per Square Meter, A/m ²
J_m	Current sheet Strength	Amperes per Square Meter, A/m ²
k_c	Carters Coefficient	-
k_d	Distribution factor	-
k_p	Pitch factor	-
k_w	Winding factor	-
K_p	Saturation Correction Coefficient	-
l_{ce}	Length of end connection wire	Meters, m
l_w	Length of copper wire	Meters, m
L_s	Length of one Stator unit	Meters, m
m	Number of Phases	-
M	Magnetomotive Force	Ampere (Turn), A
N	Turns in a coil	-

N_l	Turns per phase	-
N_c	Number of Turns per Slot	-
N_p	Number of parallel wires	-
p	Number of Poles	
P_i	Input Power	Watts, W
P_o	Output Power	Watts, W
q_l	slots per pole per phase	-
R	Stator radius of Rotary Induction Motor	Meters, m
R_l	Per phase Stator Resistance	Ohms, Ω
R_2	Per phase Rotor Resistance	Ohms, Ω
S	Slip	-
T_i	Slot Insulation Factor	Meters, m
T_{lw}	Total length of copper in stator windings	Meters, m
V_l	RMS Input Phase Voltage	Volts, V
V_r	Rotor Velocity	Meters per second, m/s
V_{yoke}	Volume of core Yoke	Cubic meter, m^3
V_{tooth}	Volume of Tooth	Cubic meter, m^3
V_{teeth}	Volume of Stator Teeth	Cubic meter, m^3
V_{iron}	Total Iron Volume	Cubic meter, m^3
V_s	Synchronous velocity	Meters per second, m/s
w_s	slot width	Meters, m
w_t	Tooth width	Meters, m
w_{tmin}	Minimum Tooth Width	Meters, m

W_{copper}	Total weight of Copper wire	Kilograms, Kg
W_{iron}	Total Iron weight	Kilograms, Kg
W_s	Width of stator or Stack width	Meters, m
W_{se}	Equivalent Stator Width or Stack width	Meters, m
W_{stator}	Total weight of one unit of SLIM Stator	Kilograms, Kg
X_l	Per-phase Stator-slot Leakage Reactance	Ohms, Ω
X_m	Per-phase Magnetizing Reactance	Ohms, Ω
Z	Unit Impedance	Ohms, Ω

GREEK SYMBOLS

α	Slot angle	Electrical Degrees, $^\circ$
ϕ	Angle between voltage and current	Electrical Degrees, $^\circ$
γ	Function of S and w_s	-
η	Efficiency	-
λ	Slot Pitch	Meters, m
μ_0	Permeability of free space	Henry (Wb/A) per meter, H/m
μ_i	Permeability of back iron	Henry (Wb/A) per meter, H/m
θ_p	Coil span	Electrical Degrees, $^\circ$
ρ_{iron}	Density of Iron	Kilograms per cubic meter, Kg/m^3
ρ_r	Volume resistivity of Aluminum	Ohm-Meter, $\Omega\text{-m}$
ρ_w	Volume resistivity of Copper	Ohm-Meter, $\Omega\text{-m}$

σ	Actual Conductivity of rotor conductor	Siemens, 1/ Ω -m
σ_e	Conductivity due to skin effect	Siemens, 1/ Ω -m
σ_{ei}	Equivalent conductivity of rotor conductor	Siemens, 1/ Ω -m
σ_i	Conductivity of back iron	Siemens, 1/ Ω -m
τ	Pole pitch	Meters, m
ω	Angular velocity	Radian per second, rad/s
Φ	Flux in a coil	Weber (V.s), Wb
Φ_p	Flux Linkage per pole	Weber (V.s), Wb

DESIGN OF A SINGLE SIDED LINEAR INDUCTION MOTOR (SLIM) USING A USER INTERACTIVE COMPUTER PROGRAM

Sarveswara Bhamidi

Dr. Robert O'Connell, Thesis Supervisor

ABSTRACT

This project studies the design of SLIM, which can be used to power capsules in a pneumatic capsule pipeline (PCP) system. The design equations of the SLIM and the equivalent circuit model are studied and discussed in detail. A SLIM of specified parameters is designed using a user-interactive MATLAB program, and then compared to a similar tubular linear induction motor (TLIM). The SLIM equations and design procedures are developed and its performance is predicted using equivalent circuit models. End effects and edge effects are neglected in this study. The SLIM design algorithm is made completely user-interactive where the user has the convenience of choosing various design parameters like the primary voltage and frequency, number of

poles, number of phases and many more.

Optimum design parameters are obtained by the iterative procedure of the design algorithm. The performance curves of the SLIM i.e., thrust and efficiency, are drawn and then analyzed for different target thrust values and rated slip. The effect of varying parameters of the SLIM such as air-gap, thickness of aluminum sheet and the number of poles on the performance of SLIM are analyzed and the results are discussed. Finally the SLIM design parameters are compared with those of a similar TLIM design of similar specifications.

CHAPTER 1

INTRODUCTION

The history of linear induction motors extends as far back as the 19th century. Although these machines have been practically forgotten for the last 30 or 40 years, there appears to be a genuine revival of interest in them. The fascinating history of these “unrolled” motors and their theory of operation are discussed in this report.

The idea of the linear induction motor is probably contemporary with the invention of the rotating field machine by Tesla, Dolivo-Doborovolsky, and Ferrari some time after 1885. However, some authors give other dates for the discovery. The idea of a linear electric motor is almost as old as that of a rotary electric motor. The first linear motor was a reluctance machine built by Charles Wheatstone in 1845, to be closely followed by a similar machine by Henry Fox Talbert. Nicola Tesla invented the induction motor in 1888. The first patent in linear induction motors was obtained by the mayor of Pittsburg in 1895. The first electromagnetic gun was undoubtedly Birkeland’s cannon of 1918, again a reluctance device, but possibly the first tubular motor using a row of simple coils energized in sequence with DC. In 1946, Westinghouse built a full-scale aircraft launcher, the “Electropult”, which was an induction motor with a moving primary. It was this machine that inspired E.R.Laithwaite to begin his own work on linear motors in the 1950’s, since when there have been rapid advances in linear induction machines for

producing standstill forces, for propelling high-speed vehicles and as accelerators for producing kinetic energy.

Linear motors potentially have unlimited applications. Linear induction motors (LIM's) alone have found application in the following general areas: conveyor systems, material handling and storage, people movers, liquid metal pumping, accelerators and launchers, machine tool operation, airport baggage handling, opening and closing drapes, operation of sliding doors and low and medium speed trains. For low speed applications both flat and tubular linear induction motors (TLIM) are suitable. The single-sided linear induction motor (SLIM) is by far the most widely used linear motor [1].

A flat or single-sided LIM i.e., a SLIM, is obtained by the imaginary process of “cutting” and “unrolling” a rotary induction motor. In practice, the primary or stator of a LIM consists of a rectangular slotted structure formed by a stack of steel laminations. Within the slots of the primary stack are laid the polyphase windings to produce the linearly traveling magnetic field, just like the rotating magnetic field in a rotary induction motor, produced by the polyphase stator windings. The secondary of the LIM, or rotor, which is an aluminum sheet (or copper), with or without a solid back iron plate, completes the magnetic circuit and creates the magnetic flux linkage across the air gap. This in turn induces a voltage on the conductive wall, which generates an eddy current in the conducting outer layer of the secondary. The interaction between the eddy current and the changing electromagnetic field generates electromagnetic thrust on the plate in the longitudinal direction of the motor.

The objective of this project was to design a SLIM of specified parameters using a user-interactive computer program, and compare it to a similar tubular linear induction motor (TLIM). The study included developing SLIM equations and design procedures and predicting its performance using equivalent circuit models. Furthermore, a user-interactive design algorithm was developed and a computer program was written in MATLAB software for the design of a SLIM as per required specifications. Optimum design parameters are obtained by the iterative procedure of the design algorithm. The values thus obtained were tabulated and then compared with those of a similar TLIM design of similar specifications. The performance curves of the SLIM are sketched and analyzed at various operating conditions. The advantages and disadvantages of using a SLIM versus a TLIM are discussed with respect to the performance curves.

This thesis, comprised of six chapters, is organized as follows. In Chapter 2, a background study of LIM history and related research in SLIM are presented. The chapter starts with the history of the LIM in various applications, then focuses on the TLIM, and finally summarizes previous research in SLIM used for various applications.

In Chapter 3, the basic principle of operation of the SLIM is discussed by analogy with the conventional rotary induction motor. All of the basic equations and parameters are explained in detail. Some of them include the power rating and rated input phase current, flux linkage and induced voltage, effective air-gap, slot and stator yoke dimensions, and SLIM magnetomotive forces. The performance of a SLIM is predicted and analyzed using the equivalent circuit approach. Thrust and efficiency are the performance parameters that are considered in this section. The equivalent circuit

parameters are determined from its developed model and then the performance parameters are determined.

In Chapter 4, from the design equations given in the previous chapter, the SLIM is designed. The design procedures and the design algorithm are discussed in detail. The iterative procedures given in the algorithm are also discussed. The designed SLIM is then compared to a similar TLIM.

In Chapter 5, the performance of a SLIM based on varying different parameters is evaluated. The design parameters of a 3.14 meter wide SLIM at specified rotor velocity are simulated and tabulated. The various characteristic curves of the designed SLIM stator and the parametric performance evaluation of SLIM design are also discussed. The effects of varying air-gap, rotor aluminum thickness and pole number on performance are also discussed in detail.

Finally, in Chapter 6, conclusions are drawn and some ideas for further study are discussed.

CHAPTER 2

LITERATURE REVIEW

Patent literature first mentions linear induction machines in 1890, only two years after the discovery of the rotary induction principle. The electric shuttle used in a weaving loom, and which employed a LIM, was developed by the Waver Jacquard and Electric Shuttle Company in England and was patented in 1895. Around 1891, the “Portelectric system”, intended for luggage transportation, was tested in Dorchester, Massachusetts [2].

The idea of a train system originated with Korda but was reinvented by Rosenfeld, Zelenay and Dulait, who actually experimented with it. The test track was electrified over a length of 400 meters and had 20 primaries which were 2.8 meters long and were gramme-wound. In 1902, Zehden applied for a French patent on an “electric traction system” and for a similar patent in the U.S. in 1907, in which he suggested dragging a train with a short primary mounted under the cars, and using a long secondary with a configuration quite similar to those that are now tested for high-speed ground transportation [3, 4, 5].

After 1910, however, and until the end of World War II, the interest in linear machines declined, with the exception of the electromagnetic gun and various

experiments on looms [6]. During the late 1940's, the Westinghouse Electric Corporation began carrying out two large-scale experiments for the U.S. Navy [7]. The apparatus known as Electropult was built for the U.S. Navy to launch aircraft. The primary winding was mounted to a wheel-supported shuttle while the slotted iron secondary served as a track on the ship deck. The secondary consisted of a squirrel cage, set flush with the ship deck. Its length was 425 meters, the useful core was 30 cm wide, and the required ac power amounted to 12000 kw. The launching run was 300 meters long, and it lasted 4 to 15 minutes, bringing the plane from rest to a take-off speed that could be as high as 360 km/h. The remaining 125 meters was used for stopping the shuttle with a reversal of the magnetic field, after the aircraft took off. Although its originators claimed that the launcher did not have the limitations in speed or capacity of the mechanical types of launching devices, prohibitive expense prevented further developments of the Electropult [8].

During this period, the development of nuclear energy led to the study of electromagnetic pumps for liquid metals, particularly sodium. The annular linear induction pump and the flat linear induction pump are similar to linear induction motors. Furthermore, a search for new ways of generating electricity led to the investigation of liquid-phase magnetohydrodynamic (MHD) generators. These include the liquid induction pumps just described, operating above synchronous speed [9].

During this same time, E.R.Laithwaite became quite enthusiastic about the linear induction motor. He directed many theses on the subject in his laboratory at Manchester University, and the first results of his work were published in the proceedings of the IEE

(London). Since then, he has published related papers in many professional journals, attracting the attention of many engineers to the subject. He analyzed linear induction motors according to their configurations and associated applications and published them in his 1966 book [10].

The LIM has a beginning and an end in the direction of travel. This feature produces an end effect that adversely influences the performance of the linear motor. This is one of the most important differences between the linear induction motor and the rotary induction motor. Hence, the longitudinal end effects that are of concern in a LIM are not a consideration for rotary motors. Yamamura [11] and Poloujadoff [12] studied the theoretical aspects of LIM in detail, especially the influence of longitudinal end effects. Both works are primarily concerned with theoretical analysis of single and double-sided linear induction motors. Nasar and Boldea [1, 13] also did extensive research on linear electric motors. The single-sided linear induction motor which is the subject of this project is well discussed in their book. The most recent book on LIMs, by Gieras [14], covers all aspects of the subject, including constructional features, applications, electromagnetic effects, and design. Linear induction motors of single-sided, double-sided, and tubular configurations are analyzed in terms of equivalent circuits and their components.

There is a wealth of literature on the analysis of linear induction motors, but very few papers that focus directly on the design of a LIM, which is the main subject of this project. A complete equivalent circuit of a linear induction motor with sheet secondary was developed by R.M.Pai and I.Boldea [15]. They derived the steady state performance

characteristics of linear induction motors have been determined using one-, two-, and three-dimensional analyses, including longitudinal end effects, transverse edge effects, and skin effects in the secondary. Furthermore, they obtained an equivalent circuit of a LIM from the field analysis, where the longitudinal-end effect, transverse-edge effect, and the skin effect are taken into account.

In 1988, a study of the causes and consequences of phase imbalance in single-sided linear induction motor was demonstrated by Anthony R. Eastham and J.F. Gieras [16]. In that paper, two methods of evaluating phase imbalance were presented. The first method, which is analytical, is based on an equivalent circuit model. The second approach, which is numerical, uses the finite-element method. The computational results were validated by comparison with test results on a single-sided LIM at Queens University. It was also shown that phase imbalance produces a reduction in both thrust and normal forces, but this effect is likely to be significant only for high-speed LIM's.

An investigation of LIM dynamic performance assessment from parameter identification was published by Zhang, Eastham and Dawson in 1993 [17]. The paper presents a reliable method of obtaining nominal parameters of an induction motor based on conventional tests, and then proposes a dynamic performance assessment scheme for linear induction motors, based on an on-line parameter updating algorithm. The experiments with a static LIM test device demonstrate its effectiveness. The verified scheme was then applied to an operational transportation LIM and it was shown that this computed real-time information can be used for control purposes.

The study of applying linear induction motors to the acceleration of large masses to high velocities was carried out by E.R.Laithwaite in 1995 [18]. The paper describes the features needed in the design of a linear induction motor that will accelerate a mass of 200 kg to 1200 m/s in a distance of 1500 m. Attention was confined to the accelerated part of the motion. Deceleration to rest in the second 1500 m of track can be approached with the same techniques. It became clear that many novel features needed to be embodied in the design and that these features extended the practice of making linear induction motors. It is believed that the techniques described and the topologies to which they relate may have wider application. This study threw light on the fundamental principles of linear induction motors in general and in particular on motors in which a number of features, generally believed to be essential to the proper design of induction devices, were discarded.

In 1997, a paper by Simone, G.A, Creppe, R.C. and de Souza, C entitled “The thrust and the relation factor K_R in linear induction machines” [19], shows a new way to establish the thrust of a linear induction machine. A new factor named the relation factor is established, which provides conditions necessary to establish the thrust and other important variables of the linear induction machines.

Recently, LIMs are being used in industry as transportation systems. In semiconductor factories dust cannot be tolerated during conveyance. A LIM which can be used in such a place was developed in 1999 [20]. This paper presents the characteristics of a two-phase levitated linear induction motor. The system is ac induction type, and its secondary conductor completely levitates and moves above a stator by non-

contact. The secondary conductor using the self-shading effect is also proposed for stable levitation. The validity of the proposed method was demonstrated by comparing the calculated results from the finite element method with the results of experiments.

The accurate modeling of a single-sided linear induction motor considering end effect and equivalent thickness, which is the thickness of aluminum sheet with a solid back iron plate, was demonstrated by Jawad Faiz in 2000 [21]. An analytical technique based on the equivalent circuit model, one dimensional (1-D) theory, and two-dimensional (2-D) field analysis is used to predict performance characteristics for the single-sided linear induction motor (SLIM). In this technique a new idea is introduced to account for the longitudinal end effect. Simulation results produced by this analytical technique have a better agreement with the experimental results than those reported in the literature. This analytical model may be used to predict the sensitivity of the performance characteristics to various parameters.

In 2002, the model suggested by Duncan for simulation of linear induction motors was modified by means of the finite-element method (FEM) [22]. The modified model covers special phenomena in linear motors such as transverse edge effect, longitudinal end effect, and saturation of back iron. The modified model first computes the level of saturation by both simple calculations and an iterative method. Then, using the FEM, it computes the equivalent circuit parameters. Finally, it uses the Duncan model to account for the end effect. The modified model thus can be used to design linear induction motors. A comparison of the simulation results based on the proposed model with experimental measurements shows the accuracy of the model.

The latest development to bring attention to the linear induction motor arose from the need for better urban and intercity mass transportation. There have been efforts to maximize improvements on conventional trains using all the refinements of modern technology. The Bay Area Rapid Transit System of San Francisco [23], the New Tokaido Line [24], and the introduction of turbine-propelled locomotives are perfect examples of systems that use LIMs. But millions of dollars are now also being allocated to develop new ground or underground vehicles that will travel at speeds so fast that wheels will be impractical. The greatest effort involving linear motors to attain ultrahigh speeds for mass transportation was studied at Rensselaer Polytechnic Institute, New York State [25].

Finally, Freight Pipeline Company (FPC) located in Columbia, Missouri, USA, has been awarded a project sponsored by the New York State Energy Research and Development Authority (NYSERDA) to study the feasibility of using the vast underground network of tunnels in New York City for freight transport by pneumatic capsule pipelines (PCP) propelled by LIMs [26].

CHAPTER 3

SLIM THEORY AND EQUATIONS

The principle of operation of a LIM is the same as that of a rotary induction motor. A linear Induction motor is basically obtained by opening the rotating squirrel cage induction motor and laying it flat. This flat structure produces a linear force instead of producing rotary torque from a cylindrical machine. LIMs can be designed to produce thrust up to several thousands of Newtons. The winding design and supply frequency determine the speed of a LIM.

The basic principle of LIM operation is similar to that of a conventional rotating squirrel-cage induction motor. Stator and rotor are the two main parts of the conventional three phase rotary induction motor. The stator consists of a balanced polyphase winding which is uniformly placed in the stator slots along its periphery. The stator produces a sinusoidally distributed magnetic field in the air-gap rotating at the uniform speed $2\omega/p$, with ω representing the network pulsation (related to the frequency f by $\omega = 2\pi f$) and p the number of poles. The relative motion between the rotor conductors and the magnetic field induces a voltage in the rotor. This induced voltage will cause a current to flow in the rotor and will generate a magnetic field. The interaction of these two magnetic fields will produce a torque that drags the rotor in the direction of the field. This principle would not be modified if the squirrel cage were replaced by a continuous sheet of conducting

material.

3.1. SLIM Concept and Equations

From the induction motor principle explained above, we obtain a linear motor if we imagine cutting and unrolling the motor, as shown in Fig. 3-1, causing the motor to have a linear motion.

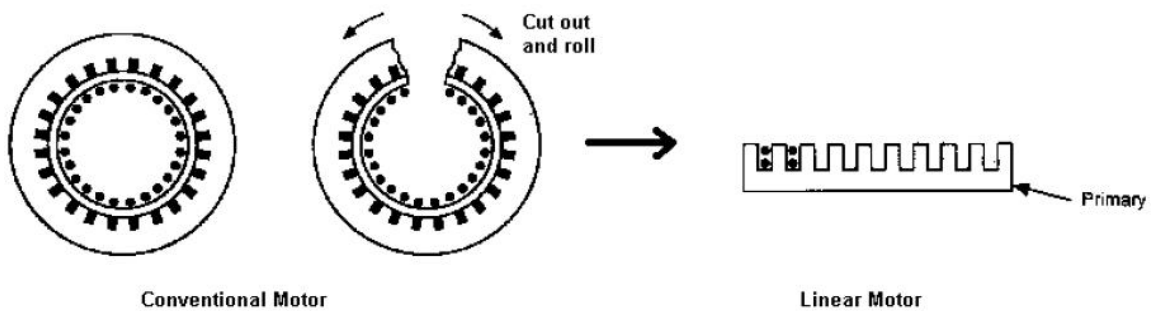


Fig 3-1 Imaginary process of unrolling a conventional motor to obtain a LIM

Instead of rotating flux, the primary windings now create flux in a linear fashion. The primary field interacts with the secondary conductors and hence exerts a force on the secondary. Generally, the secondary is made longer than the primary to make maximum use of the primary magnetic field [25].

As stated earlier, there should be relative motion between the conductor and the magnetic lines of flux, in order for a voltage to be induced in the conductor. That's why induction motors, normally operate at a speed V_r that is slightly less than the synchronous velocity V_s . Slip is the difference between the stator magnetic field speed and the rotor speed. Slip is the relative motion needed in the induction motor to induce a voltage in the

rotor, and it is given by

$$S = \frac{V_s - V_r}{V_s} \quad (3.1)$$

The SLIM synchronous velocity V_s is the same as that of the rotary induction motor, given by

$$V_s = \frac{2\omega R}{p} = 2f\tau \quad (3.2)$$

where, R is the stator radius of the rotary induction motor, as shown in Fig 3-2. It is important to note that the linear speed does not depend upon the number of poles but only on the pole pitch.

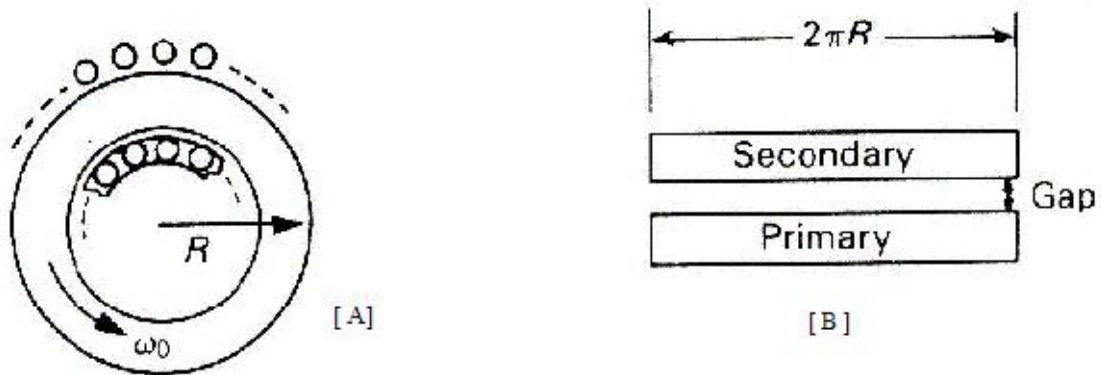


Fig 3-2 Radius of a rotary induction motor and length of a SLIM

The parameter τ is the distance between two neighboring poles on the circumference of the stator, called pole pitch, defined as [27]

$$\tau = \frac{2\pi R}{p} \quad (3.3)$$

The stator circumference of the rotary induction motor, $2\pi R$, in (3.3) is equal to the length of the SLIM stator core, L_s as shown in figure 3-2. Therefore, the pole pitch of a SLIM is

$$\tau = \frac{2\pi R}{p} = \frac{L_s}{p}. \quad (3.4)$$

If the velocity of the rotor is V_r , then the slip of a SLIM can be defined as

$$S = \frac{V_s - V_r}{V_s}. \quad (3.5)$$

The air-gap shown in Fig. 3-2[b] is the clearance between the rotor wall and the SLIM stator in a PCP-SLIM system.

3.1.1. The concept of current sheet

As mentioned earlier, the stator of an induction machine consists of several coils, each having many turns of wires – the windings – embedded in slots in laminated iron. The current carried by the windings can be replaced by a fictitious and infinitely thin layer of current distributed over the surface of the stator facing the air gap. This current is called the “current sheet.” The current sheet produces the same sinusoidal magnetomotive force (mmf) in the air gap as that produced by the conductors.

The current sheet strength, i.e, the amount of current per unit stator length (L_s) in a current sheet of a SLIM, can be calculated as in Nasar and Boldea [30] as follows:

$$J_m = \frac{2\sqrt{2}mk_w N_c I_1}{L_s} \quad (3.6)$$

In (3.6), J_m is the current sheet strength (amp/meter); m is the number of phases of the motor; k_w is the winding factor, defined below; N_c is the number of turns per slot; I_1 is

the RMS value of the input current; L_s is the length of one section of the stator of the LIM, which is equivalent to the circumference of a rotary motor, namely, $L_s = 2\pi R = p\tau$.

The winding factor, k_w , is defined as the product of pitch factor k_p and the distribution factor k_d .

$$k_w = k_p k_d \quad (3.7)$$

where k_p is the pitch factor of the coil, which is given by

$$k_p = \sin\left(\frac{\theta_p}{2}\right) \quad (3.8)$$

where θ_p is the coil span in electrical degrees. In (3.7), k_d is the breadth or distribution factor given by

$$k_d = \frac{\sin\left(\frac{q_1\alpha}{2}\right)}{q_1 \sin\left(\frac{\alpha}{2}\right)} \quad (3.9)$$

where α is the slot angle in electrical degrees given as

$$\alpha = \frac{\pi}{mq_1} . \quad (3.10)$$

One pole pitch is equal to 180 electrical degrees. So, in a full pitch coil where the coil span is equal to one pole pitch, the pitch factor becomes one. Therefore, the winding factor for the fundamental harmonic of a full pitch coil can be obtained by substituting (3.10) in (3.9) resulting in (3.11) [33].

$$k_w = \frac{\sin\left(\frac{\pi}{2m}\right)}{q_1 \sin\left(\frac{\pi}{2mq_1}\right)} \quad (3.11)$$

In (3.11), q_1 is the number of slots-per-pole-per-phase in the stator iron core.

3.1.2. Power Rating and Rated Input Phase Current

The electrical power input to the stator windings is converted into useful mechanical power by the principle of electrical induction, as explained before, and the expressions relating to the power balance are derived as follows.

The power input to the stator windings is given by

$$P_i = mV_1I_1 \cos \phi, \quad (3.12)$$

where m is the number of electrical phases, V_1 and I_1 are the RMS input phase voltage and current, respectively, and ϕ is the power factor, which is the phase angle between V_1 and I_1 . Included in this input power is a component for the copper losses in the stator windings, and a component for the iron losses in the stator core and teeth. The remaining input power is transferred to the rotor through the magnetic field of the air-gap. Neglecting the rotor conductor losses and friction and windage losses, the power transferred to the rotor can be equated to the mechanical power developed by the rotor. The total mechanical power developed by the rotor of the SLIM is given by [29]

$$P_o = F_s V_r, \quad (3.13)$$

where F_s is the electromagnetic thrust generated on the rotor by the stator, and, as stated before, V_r is the speed of the rotor. The SLIM efficiency η is calculated from

$$\eta = \frac{P_o}{P_i} = \frac{F_s V_r}{m V_1 I_1 \cos \phi} . \quad (3.14)$$

From (3.14), we initially assume a suitable operating value for $\eta \cos \phi$, and then the rated input phase current can be estimated from

$$I_1 = \frac{F_s V_r}{m V_1 \eta \cos \phi} . \quad (3.15)$$

3.1.3 Flux Linkage and Induced Voltage

Consider a coil of N turns carrying a current of I amperes and let Φ be the resulting flux linking the coil. If we assume that the flux density Φ in the air-gap is purely sinusoidal, then it can be expressed as

$$\Phi = \Phi_p \sin \omega t , \quad (3.16)$$

where Φ_p is the amplitude of the flux linkage per pole. By flux linkage, we mean the product of flux in webers and the number of turns with which the flux is linked. The induced voltage per turn in the above coil due to a change of flux is given by the first derivative of the above equation, (3.16) and is represented as

$$e = \frac{d\Phi}{dt} = \omega \Phi_p \cos \omega t . \quad (3.17)$$

The RMS value of e is

$$E_1 = \frac{2\pi}{\sqrt{2}} f \Phi_p = \sqrt{2} \pi f \Phi_p . \quad (3.18)$$

If the coil has N_1 turns per phase and a winding factor k_w , 3.18 becomes

$$E_1 = \sqrt{2} \pi f \Phi_p k_w N_1 \quad (3.19)$$

Magnetic flux density is found by dividing the flux by the cross sectional area. Hence, the

average air-gap magnetic flux density, $B_{g\text{avg}}$ can be determined as

$$B_{g\text{avg}} = \frac{\Phi_p P}{L_s W_s}, \quad (3.20)$$

where W_s is the width of SLIM stator iron core, and L_s is the length of stator and p is the number of poles. We assume that the flux produced in the air-gap is sinusoidal, having a maximum of $B_{g\text{max}}$. Hence, the average value of the rectified magnetic flux density is

$$B_{g\text{avg}} = \frac{2}{\pi} B_{g\text{max}}. \quad (3.21)$$

3.1.4. Equations for SLIM slot Geometry

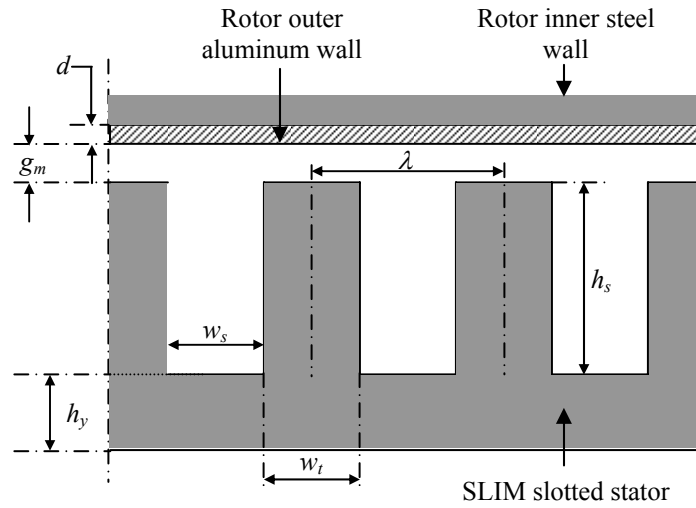


Fig 3-3 SLIM geometry [29].

The air-gap is a very important parameter in a machine. The effective air-gap g_e of the SLIM is different from the physical air-gap, g_m , because of the slotted structure of the stator, as shown in Fig. 3-3. According to Gieras [14],

$$g_e = k_c g_0. \quad (3.22)$$

where g_0 is the magnetic air-gap, given by

$$g_0 = g_m + d . \quad (3.23)$$

where d is the thickness of the conducting layer on the surface of the rotor, and k_c is known as Carter's coefficient, given by

$$k_c = \frac{\lambda}{\lambda - \gamma g_0} . \quad (3.24)$$

The parameter λ in (3.24) is the slot pitch, which is the distance between the centers of two consecutive teeth, given by

$$\lambda = \frac{\tau}{mq_1} . \quad (3.25)$$

The quantity γ in (3.24) can be expressed as [29]

$$\gamma = \frac{4}{\pi} \left[\frac{w_s}{2g_0} \arctan\left(\frac{w_s}{2g_0}\right) - \ln \sqrt{1 + \left(\frac{w_s}{2g_0}\right)^2} \right] . \quad (3.26)$$

Slot pitch is the sum of slot width and tooth width and hence the slot width can be calculated with

$$w_s = \lambda - w_t \quad (3.27)$$

where, w_t is the tooth width. To avoid magnetic saturation in the stator teeth, there is a minimum value of tooth width $w_{t\min}$, which depends on the maximum allowable tooth flux density, $B_{t\max}$. The quantity $w_{t\min}$ can be determined from [29]

$$w_{t\min} = \frac{\pi}{2} B_{g\text{avg}} \frac{\lambda}{B_{t\max}} . \quad (3.28)$$

The stator slot depth h_s shown in Fig. 3-3, can be calculated from

$$h_s = \frac{A_s}{w_s} \quad (3.29)$$

where, A_s is the cross-sectional area of a slot. Generally, 30% of the area of the slot is filled with insulation material. Therefore, A_s can be calculated from

$$A_s = \frac{10}{7} N_c A_w \quad (3.30)$$

where N_c is the number of turns per slot, determined from

$$N_c = \frac{N_1}{pq_1}. \quad (3.31)$$

The variable A_w in (3.30) is the area of cross section of a conductor winding without insulation, which can be obtained with

$$A_w = \frac{I_1}{J_1} \quad (3.32)$$

where, I_1 is the rated input phase current defined in (3.15), and J_1 is the stator current density. The value of J_1 , which depends on the machine output power and the type of cooling system, is assumed to be 6A/m^2 at the beginning of the program and later modified appropriately.

The yoke height of the stator core h_y [31] is the portion of the core below the teeth, as shown in Fig. 3-3. If it is assumed that the flux in the yoke is one-half of the flux in the air-gap, then it can be expressed as [29]

$$h_y = \frac{\Phi_p}{2B_{y\max} W_s}. \quad (3.33)$$

3.2. Forces in LIM

The main forces involved with the LIM are thrust, normal force, and lateral force, as shown in Fig 3-4. This project is interested in thrust and its relation to other variable parameters. The normal force is perpendicular to the stator in the z-direction. Lateral forces are undesirable forces which are developed in a SLIM because of the orientation of the stator.

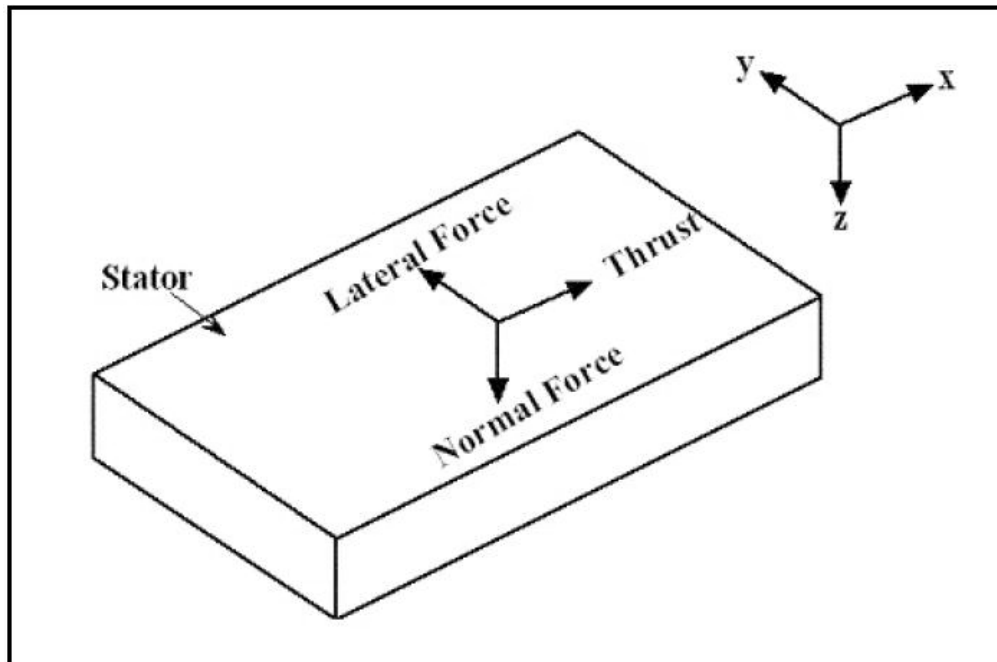


Fig 3-4. Forces in a LIM

3.2.1. Thrust

Under normal operations, the LIM develops a thrust proportional to the square of the applied voltage, and this reduces as slip is reduced similarly to that of an induction motor with a high rotor resistance.

From (3.13), the amount of thrust produced by a LIM is as follows:

$$F_s = \frac{P_o}{V_c} \quad (3.34)$$

where P_o is the mechanical power transmitted to the rotor or the output power and V_c is the linear speed of the rotor.

3.2.2. Normal Forces

In a double-sided linear induction machine (DLIM) configuration, the reaction plate is centrally located between the two primary stators. The normal force between one stator and the reaction plate is ideally equal and opposite to that of the second stator and hence the resultant normal force is zero. Therefore, a net normal force will only occur if the reaction plate (secondary) is placed asymmetrically between the two stators. This force tends to center the reaction plate.

In a SLIM configuration, there is a rather large net normal force between the primary and secondary because of the fundamental asymmetrical topology. At synchronous speed, the force is attractive and its magnitude is reduced as the speed is reduced. At certain speeds the force will become repulsive, especially at high-frequency operation.

3.2.3. Lateral Forces

As shown in Fig 3.4, lateral forces act in the y- direction, perpendicular to the movement of the rotor. Lateral forces make the system unstable. These occur due to the asymmetric positioning of the stator in a LIM. Generally, small displacements will only

result in very small lateral forces. These forces are a matter of concern in high frequency operation ($\gg 60\text{Hz}$) where they increase in magnitude. A set of guided mechanical wheel tracks is sufficient to eliminate a small lateral force.

3.3. SLIM Performance from Equivalent Circuit Model

For the analysis and design of a SLIM having negligible end-effects, the per-phase conventional equivalent circuit shown in Fig 3-5 may be used. The circuit components are determined from the SLIM parameters. The SLIM performances to be determined are thrust and efficiency.

3.3.1. Equivalent Circuit Models and Components

The approximate equivalent circuit of a LIM is presented as shown in Fig. 3-5. This circuit is on a per phase basis. The core losses are neglected because a realistic airgap flux density leads to moderate flux densities in the core and hence, rather low core losses. Skin effect is small at rated frequency for a flat linear induction motor with a thin conductive sheet on the secondary. Therefore, equivalent rotor inductance is negligible [15]. The remaining non-negligible parameters are shown in Fig 3-5 and are discussed below.

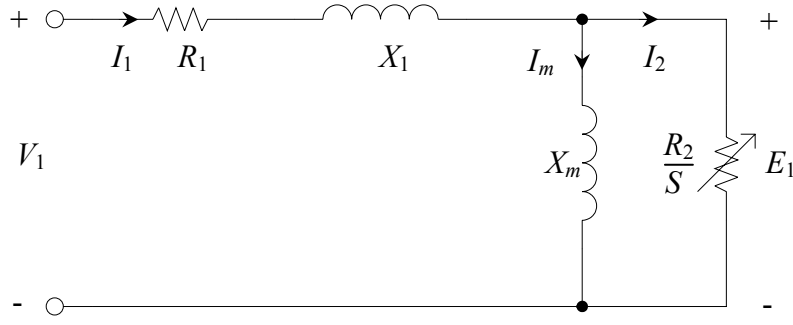


Fig. 3-5 Per-phase SLIM equivalent circuit.

i) Per-phase stator resistance R_l

This is the resistance of each phase of the SLIM stator windings. R_1 is calculated from

$$R_1 = \rho_w \frac{l_w}{A_{wt}} \quad (3.35)$$

where, ρ_w is the volume resistivity of the copper wire used in the stator winding, l_w is the length of the copper wire per phase, and A_{wt} is the cross-sectional area of the wire as given in (3.32). The length of the copper wires l_w is calculated from

$$l_w = N_1 l_{w1} \quad (3.36)$$

where

$$l_{w1} = 2(W_s + l_{ce}), \quad (3.37)$$

is the mean length of one turn of the stator winding per phase and l_{ce} is the length of end connection given by

$$l_{ce} = \frac{\theta_p}{180^\circ} \tau \quad (3.38)$$

ii) Per-phase stator-slot leakage reactance X_l

The flux that is produced in the stator windings is not completely linked with the rotor conductors. There will be some leakage flux in the stator slots and hence stator-slot leakage reactance X_1 . This leakage flux is generated from an individual coil inside a stator slot and caused by the slot openings of the stator iron core. In a SLIM stator having open rectangular slots with a double-layer winding[†], X_1 can be determined from [1]

$$X_1 = \frac{2\mu_0\pi f \left[\left(\lambda_s \left(1 + \frac{3}{p} \right) + \lambda_d \right) \frac{W_s}{q_1} + \lambda_e l_{ce} \right] N_1^2}{p} \quad (3.39)$$

where

$$\lambda_s = \frac{h_s (1 + 3k_p)}{12w_s}, \quad (3.40)$$

k_p is the pitch factor given by (3.8). Also,

$$\lambda_e = 0.3(3k_p - 1), \quad (3.41)$$

and

$$\lambda_d = \frac{5 \left(\frac{g_e}{w_s} \right)}{5 + 4 \left(\frac{g_0}{w_s} \right)}. \quad (3.42)$$

[†] Generally, the stator winding is either single-layer or double-layer windings. In a single-layer winding, one side of a coil called a coil side occupies an entire slot, while there are two different coil sides of different phases in any one slot in a double-layer winding.

iii) Per-phase magnetizing reactance X_m

The per-phase magnetizing reactance, X_m , is shown in Fig 3-5 and is given by [1]

$$X_m = \frac{24\mu_0\pi f W_{se} k_w N_1^2 \tau}{\pi^2 p g_e} \quad (3.43)$$

where k_w is the winding factor defined as in (3.7) , g_e is the equivalent air gap given by (3.22) and W_{se} is the equivalent stator width given as

$$W_{se} = W_s + g_0 . \quad (3.44)$$

iv) Per-phase rotor resistance R_2

The per-phase rotor resistance R_2 is a function of slip, as shown in Fig. 3-5. R_2 can be calculated from the goodness factor G and the per-phase magnetizing reactance X_m as

$$R_2 = \frac{X_m}{G} \quad (3.45)$$

where the goodness factor is defined as [1]

$$G = \frac{2\mu_0 f \tau^2}{\pi \left(\frac{\rho_r}{d}\right) g_e} . \quad (3.46)$$

In (3.46), ρ_r is the volume resistivity of the rotor conductor outer layer, which is aluminum here.

From the equivalent circuit shown in Fig. 3-5, the magnitude of the rotor phase current I_2 can be seen to be

$$I_2 = \frac{X_m}{\sqrt{\left(\frac{R_2}{S}\right)^2 + X_m^2}} I_1. \quad (3.47)$$

By substituting the value of R_2 from (3.45), the rotor phase current I_2 becomes

$$I_2 = \frac{I_1}{\sqrt{\frac{1}{(SG)^2} + 1}}. \quad (3.48)$$

3.4. Thrust and Efficiency

As explained earlier, the input power to the stator windings is utilized in producing useful mechanical power which is exerted on the rotor and to account for the rotor copper losses. In terms of the equivalent circuit components, the mechanical power developed by the rotor is the power transferred across the air-gap from the stator to the rotor ($mI_2^2 \frac{R_2}{S}$) minus the rotor copper loss ($mI_2^2 R_2$) [29], or

$$P_o = mI_2^2 \frac{R_2}{S} - mI_2^2 R_2 = mI_2^2 R_2 \left(\frac{1-S}{S}\right). \quad (3.49)$$

Using the equations for P_o from (3.13) and $V_r = V_s(1-S)$ from (3.1) in (3.49), the electromagnetic thrust generated by the SLIM stator is

$$F_s = \frac{mI_2^2 R_2}{V_s S}. \quad (3.50)$$

This is the most general form of expressing electromagnetic thrust for a SLIM determined from the rotor phase current I_2 . However, considering the per-phase SLIM equivalent circuit as shown in Fig. 3-5, where the core losses are neglected, F_s can be

expressed in terms of stator phase current I_1 . Substituting (3.48) into (3.50), the SLIM electromagnetic thrust becomes [28]

$$F_s = \frac{mI_1^2 R_2}{\left[\frac{1}{(SG)^2} + 1 \right] V_s S} . \quad (3.51)$$

The SLIM input active power is the summation of the output power and the copper losses from the stator and rotor,

$$P_i = P_o + mI_1^2 R_1 + mI_2^2 R_2 \quad (3.52)$$

where, $mI_1^2 R_1$ is the stator copper loss [32]. Substituting (3.49), and (3.51) into (3.52) yields

$$P_i = F_s V_s + mI_1^2 R_1 . \quad (3.53)$$

The efficiency of the SLIM is found by calculating the ratio of (3.49) and (3.53), i.e.

$$\eta = \frac{P_o}{P_i} \quad (3.54)$$

3.5. Edge effects due to secondary overhangs

In a LIM, the width of the primary stack is usually less than the width of the secondary plate resulting in a physical feature called transverse edge effects. Due to this, transverse and longitudinal components of current densities exist, consequently increasing the secondary resistance R_2 by a multiplicative factor k_{tr} , and a reducing the magnetizing reactance by a multiplicative factor k_{im} where

$$k_{tr} = \frac{k_x^2}{k_R} \frac{1 + \left(\frac{SGk_R}{k_x} \right)^2}{1 + S^2G^2} \geq 1 \quad (3.55)$$

$$k_{im} = \frac{k_R}{k_x} k_{tr} \leq 1 \quad (3.56)$$

$$k_R = 1 - \operatorname{Re} \left[(1 - jSG) \frac{2\lambda_t}{\alpha W_s} \tanh \left(\frac{\alpha W_s}{2} \right) \right] \quad (3.57)$$

$$k_x = 1 + \operatorname{Re} \left[(SG + j) \frac{2SG\lambda_t}{\alpha W_s} \tanh \left(\frac{\alpha W_s}{2} \right) \right] \quad (3.58)$$

$$\lambda_t = \frac{1}{\left[1 + \sqrt{1 + jSG} \tanh \left(\frac{\alpha W_s}{2} \right) \tanh \frac{\pi}{\tau} \left(c - \frac{W_s}{2} \right) \right]} \quad (3.59)$$

$$\alpha = \frac{\pi}{\tau} \sqrt{1 + jSG} \quad (3.60)$$

$$k_{sk} = \frac{2d}{d_s} \left[\frac{\sinh(2d/d_s) + \sin(2d/d_s)}{\cosh(2d/d_s) - \sin(2d/d_s)} \right] \quad (3.61)$$

$$k_p \approx \frac{\mu_0 \tau^2}{\pi^2} \left(\frac{1}{\mu_i \delta_i g_0 k_c} \right) \quad (3.62)$$

$$\delta_i = \text{Re} \left\{ \frac{1}{\left[\frac{\pi^2}{\tau^2} + j2\pi f_1 \mu_i \frac{S\sigma_i}{k_{tri}} \right]^{1/2}} \right\} \quad (3.63)$$

$$K_{tri} \approx \frac{1}{\left[1 - \frac{2\tau}{\pi W_s} \tanh\left(\frac{\pi W_s}{2\tau}\right) \right]} \quad (3.64)$$

$$G = \frac{2\mu_0 f_1 \sigma_e \tau^2 d}{\pi g_0 k_1 k_{sk} k_c (1 + k_p)} \quad (3.65)$$

$$g_{ei} = \frac{k_1 k_c}{k_{tm}} (1 + k_p) g_0 \quad (3.66)$$

$$\sigma_{ei} = \frac{\sigma}{k_{sk} k_{tr}} + \frac{\sigma_i \delta_i}{k_{tri} d} \quad (3.67)$$

$$G_{ei} = \frac{2\mu_0 f_1 \tau^2 \sigma_{ei} d}{\pi g_{ei}} \quad (3.68)$$

In summary, the main consequences of transverse edge effects appear in the forms of:

- an increase in secondary resistivity
- a tendency toward lateral instability
- a distortion of air gap fields, and
- a deterioration of the LIM performance, due to the first three factors.

Considering the edge effects, the equivalent circuit parameters of a SLIM can be written as follows [1]:

The factor g_e in the magnetizing reactance X_m is replaced by g_{ei} and the goodness factor G in the secondary resistance R_2 is replaced by G_{ei} so that

$$X_m = \frac{24\mu_0\pi f W_s K_w N_1^2 \tau}{\pi^2 p g_{ei}} \quad (3.69)$$

$$R_2 = \frac{X_m}{G_{ei}} \quad (3.70)$$

The primary phase resistance R_1 and leakage reactance X_1 are given by the following expressions:

$$R_1 = \frac{\rho_w (2W_s + 2l_{ce}) J_1 N_1}{I_1'} \quad (3.71)$$

$$X_1 = \frac{8\mu_0\pi f \left[\left(\lambda_s \left(1 + \frac{3}{p} \right) + \lambda_d \right) \frac{W_s}{q_1} + \lambda_e l_{ce} \right] N_1^2}{p} \quad (3.72)$$

where λ_s and λ_e are given by (3.40) and (3.41) respectively and

$$\lambda_d = \frac{5 \left(\frac{g_{ei}}{w_s} \right)}{5 + 4 \left(\frac{g_0}{w_s} \right)} \quad (3.73)$$

where g_{ei} is the equivalent air-gap given by (3.66).

The goodness factor is now given by

$$G = \frac{2\mu_0 f \tau^2}{\pi \left(\frac{\rho_r}{d} \right) g_e} \quad (3.74)$$

All specific phenomena are incorporated in g_{ei} and σ_{ei} , which are functions of primary current I_1 and slip frequency $s\omega$. Further, for low speed LIMs, the expression of thrust and normal force become simplified. Thus, the total thrust F_s may be written as

$$F_s = \frac{3I_2^2 R_2}{S2\mathcal{f}_1} = \frac{3I_1^2 R_2}{S2\mathcal{f}_1 \left[\left(\frac{1}{SG_{ei}} \right)^2 + 1 \right]}. \quad (3.75)$$

Neglecting the iron losses, the efficiency η and power factor $\cos \phi$ are:

$$\eta = \frac{F_s 2\mathcal{f}_1 (1-S)}{F_s 2\mathcal{f}_1 + 3R_1 I_1^2} \quad (3.76)$$

$$\cos \phi = \frac{F_s 2\mathcal{f}_1 + 3R_1 I_1^2}{3V_1 I_1} \quad (3.77)$$

The normal force F_n is composed of an attraction component and a repulsion component.

The final expression is [1]:

$$F_n = W_{se} \frac{p\tau^3}{\pi^2} \frac{\mu_0 J_m^2}{g_{ei}^2 (1+S^2 G_{ei}^2)} \left[1 - \left(\frac{\pi}{\tau} g_e S G_{ei} \right)^2 \right] \quad (3.78)$$

In the low speed region, the normal force is attractive (positive), but for high speeds, it may become repulsive (negative).

CHAPTER 4

DESIGN OF SLIM USING USER-INTERACTIVE PROCEDURE

The PCP-SLIM system consists of multiple SLIM stator units which are identical and connected physically in series, but electrically in parallel. These SLIM stator units power the capsules in this system. In this section, a single stator unit is designed using the equations presented in Chapter 3. Various SLIM winding configurations are discussed and then the design procedures and the design algorithm of the SLIM are presented and discussed. The iterative procedures given in the algorithm are also discussed.

4.1 Winding Configurations of a SLIM

There are many winding arrangements possible for a LIM. Prominent among them are the single layer, double layer and the triple layer winding configurations. This project is interested in the feasibility of single layer and double layer winding configurations in LIM's.

4.1.1 Single layer windings

The number of coils in a single layer winding is one-half the number of slots available, because each coil side completely occupies one slot. Each slot contains one coil side only in a single layer winding configuration, as shown in Fig. 4-1.

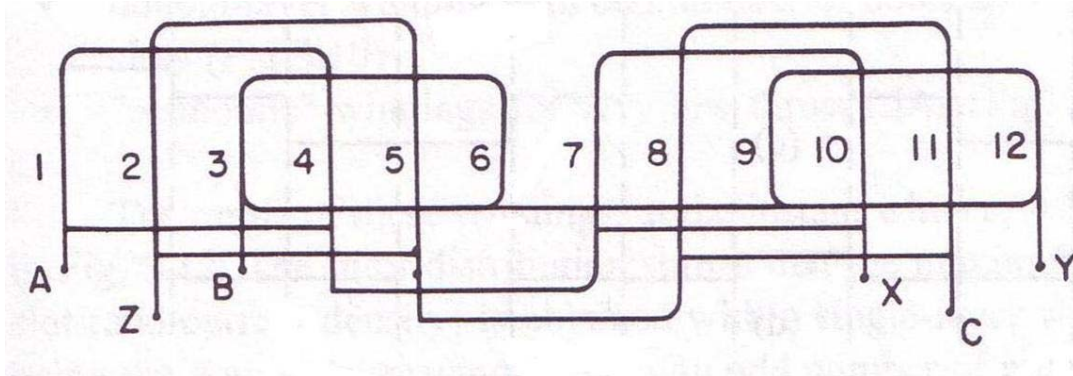


Fig. 4-1 Single layer winding configuration for a 4 pole, 3 phase, 1 slot per pole per phase, SLIM

The approximate flux density distribution of single layer windings is obtained by adding the contributions of all the three phases A, B, C as shown in figure 4-2.

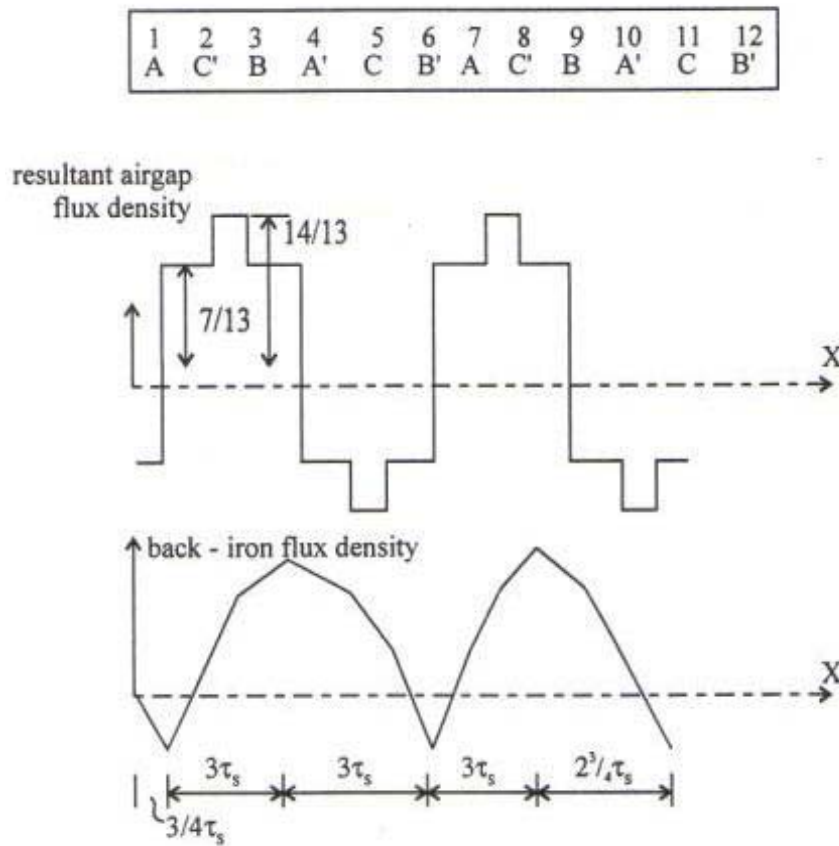


Figure 4-2 Flux distribution and back-iron density of a single layer winding.

These are quite generally used in small single phase motors because of their convenience in coil assembly. Single layer windings also eliminate the need for coil-coil insulation in slots since there is only one coil per slot.

4.1.2 Double Layer windings

The armatures of nearly all synchronous generators and motors, and most induction motors above a few kilowatts, are wound with double-layer windings. In a double layer winding, there are two sets of windings of different phases placed in the same slot, except the end slots, as shown in Fig. 4-3 [34]. Each coil has two sides. The end of each coil or its second coil side is placed below the start of the adjacent coil or its first coil side. This ensures that the windings are placed identically with respect to each other. This winding configuration results in a balanced arrangement with all three phases carrying the same amount of current. The number of turns in each coil and the parallel arrangements depends on the supply current and the size of each slot.

It is possible to construct a winding with a coil pitch less than the pole pitch. When the span from center to center of the coil, which constitutes a phase belt, is less than the pole pitch, the winding as a whole is said to be a fractional-pitch winding. Fractional pitch windings are extensively used, particularly with two layer windings because they reduce harmonics in the voltage wave and produce a more nearly sinusoidal current waveform than with full-pitch windings. They also give a saving in the amount of copper used in the overhang and the greater stiffness of the coils due to shorter end connections. The fractional-pitch, double layer winding having a coil pitch equal to one-

third the pole pitch is shown in the Figure 4-3.

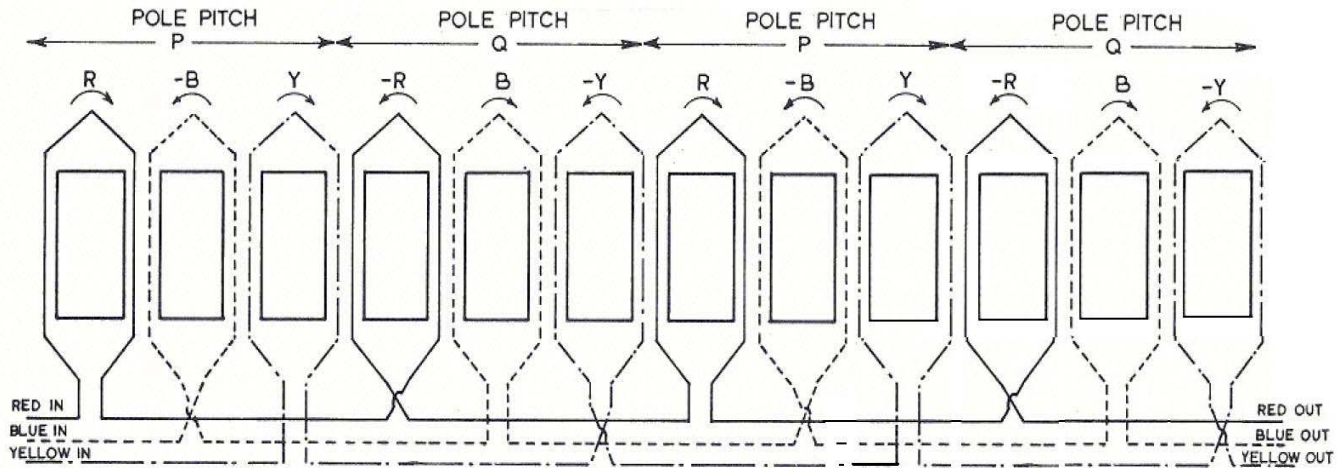


Figure 4-3 Fractional-pitch, Double layer winding for a 4 pole, 3 phase, 1 slot per pole per phase SLIM whose coil span is one-third the pole pitch.

Figure 4-4 illustrates a fractional-pitch double layer winding for a 3 phase, 4 pole, $7/6$ slots per pole per phase SLIM whose coil span is two-thirds the pole pitch. It can be seen that this winding configuration needs 14 slots compared to 12 slots in the previous arrangement as shown in Figure 4-3.

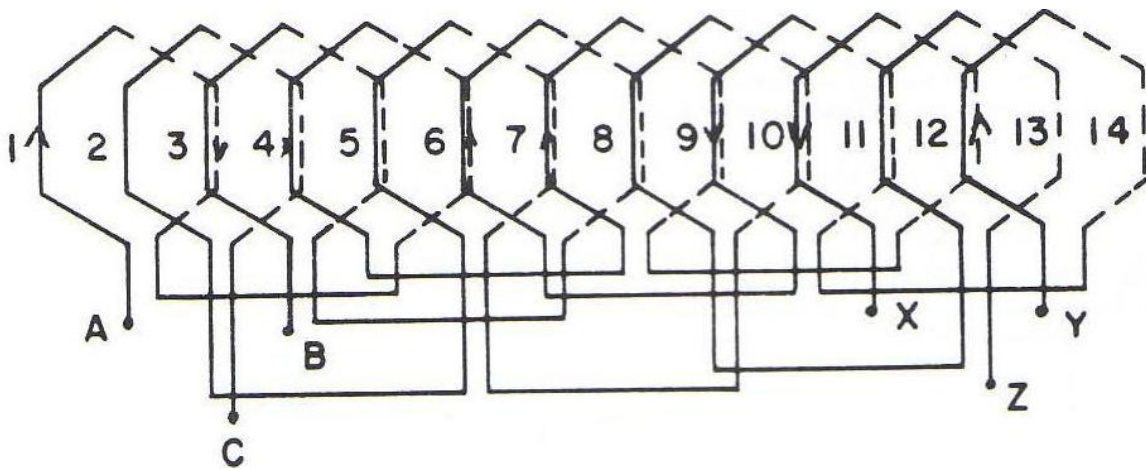


Figure 4-4 Fractional pitch, Double layer winding for a 4 pole, 3 phase, $7/6$ slot per pole per phase SLIM whose coil span is two-thirds the pole pitch.

The full-pitch, double layer winding arrangement for a 5 pole, 3 phase, 1 slot per pole per phase SLIM can be as shown in figure 4-5. The approximate flux density distribution is also shown by summing up the flux produced by individual phases. The back-iron density is also shown.

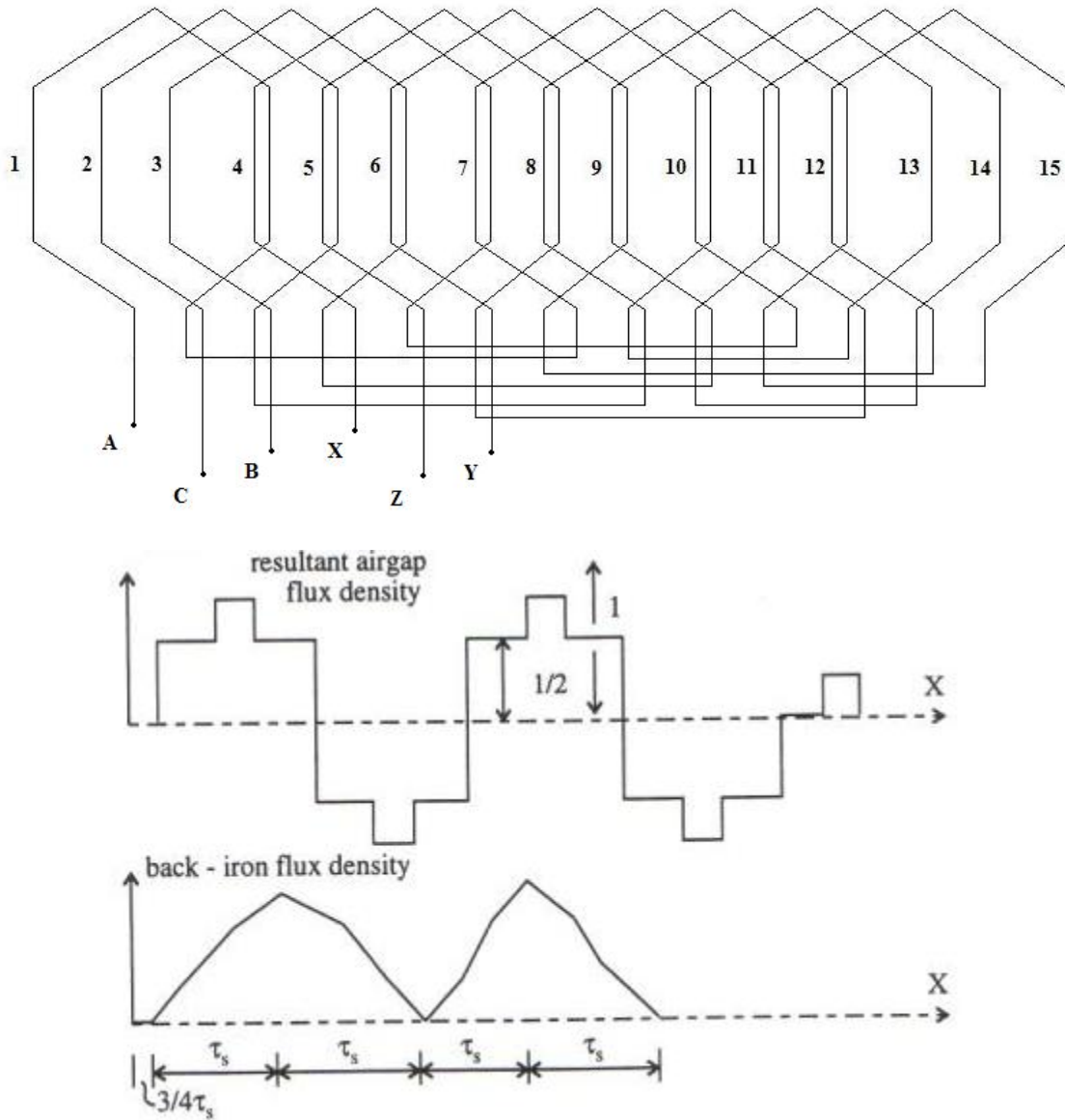


Figure 4-5 Full-pitch, double layer winding for a 5 pole, 3 phase, 1 slot per pole per phase SLIM

The advantages and disadvantages of these windings are related to the manufacturing costs and the capacity for producing an air-gap field distribution approaching a purely sinusoidal wave. The double layer winding utilizes double the number of coils than a single layer winding but it produces a very good forward traveling wave of fewer harmonics components than its counterpart. Thus, there is a tradeoff between cost and performance in choosing the type of winding for a SLIM. In high-thrust applications, the double layer winding is most suitable. In general, it may be said that modern practice favors the double-layer winding except where the slot openings would be large compared with the length of the air-gap, as in high voltage induction motors [35].

In the remainder of this chapter, the design of the SLIM with a single layer winding is discussed in detail. The results of various designs of SLIM are tabulated as shown in Tables 4-4 through 4-9. The flow chart for the SLIM design algorithm is as shown in Fig. 4-6. This is similar to the flow chart for the design of TLIM proposed by Plodpradishta [29].

4.2. SLIM Stator Unit Design

The SLIM stator unit is designed according to the flow chart shown in Fig. 4-6. The step by step procedure of the design is described below.

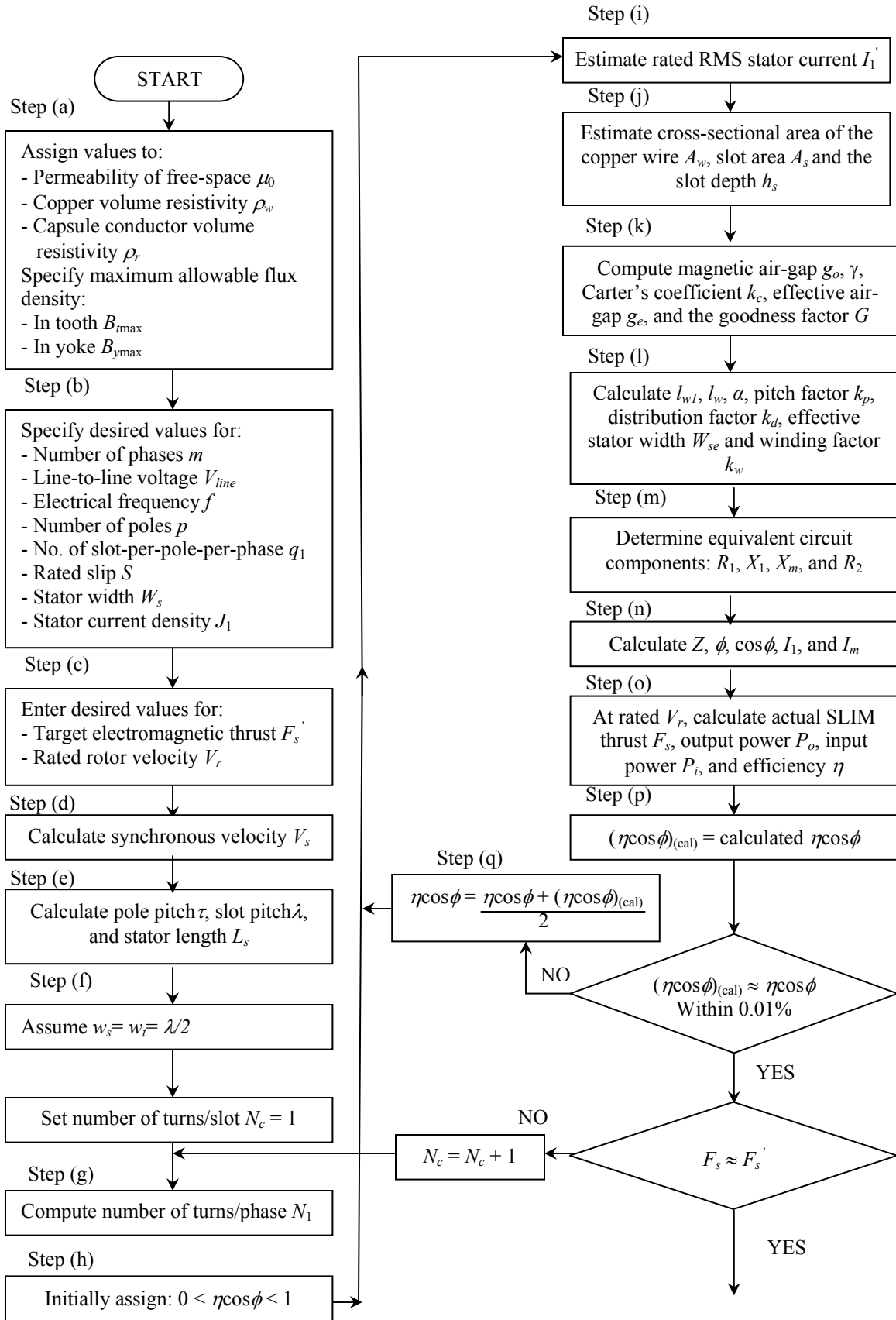
Step (a) First of all, we assign constant values for the permeability of free-space, μ_0 , copper volume resistivity, ρ_w , and capsule conductor volume resistivity, ρ_r . We also

specify the maximum allowable flux density in a stator tooth, B_{tmax} and in the stator yoke, B_{ymax} . These constant values can be tabulated as shown in table 4-1.

Table 4-1 Necessary Constants in the design of SLIM

CONSTANT	VALUE
Permeability of free-space (H/m), μ_0	$4\pi*10^{-7}$
Copper volume resistivity (Ω -m), ρ_w	$19.27*10^{-9}$
Capsule conductor volume resistivity (Ω -m), ρ_r	$28.85*10^{-9}$
Maximum tooth flux density (Wb/m^2), B_{tmax}	1.6
Maximum yoke flux density (Wb/m^2), B_{ymax}	1.9

Step (b) The user interactive program allows us to enter the desired or specified values of some of the parameters needed for the design of the SLIM. The user chooses the number of electrical phases, m , RMS line-to-line voltage, V_{line} , electrical frequency, f , the number of poles, p , the number of slots per pole per phase, q_1 , the slip of operation, S , the stator width, W_s , the size of the air-gap g_m , the coil span θ_p , the rotor outer conductor thickness d , and the stator current density J_1 . The values used in this project for the above stated parameters are as listed in Table 4-2.



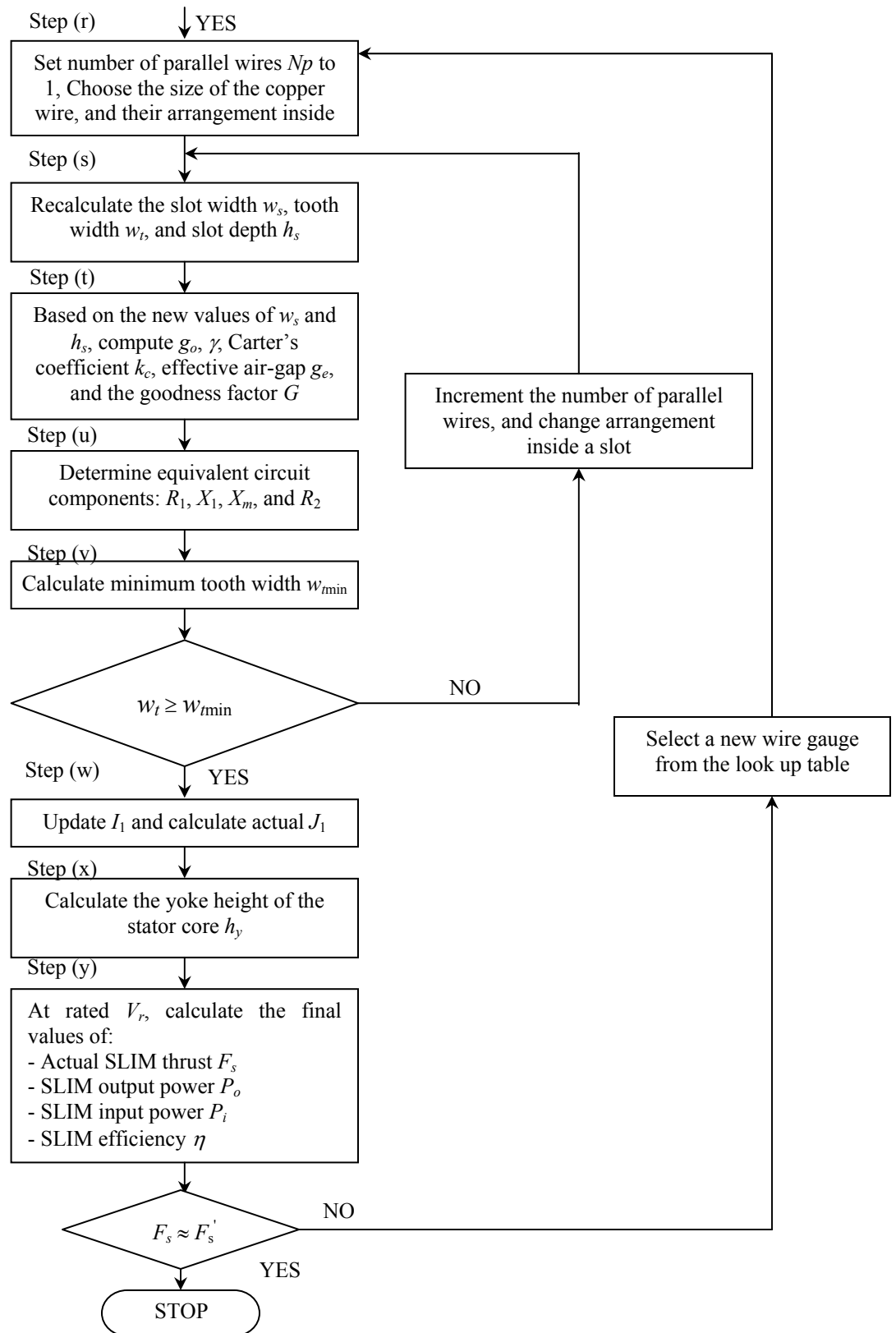


Fig 4-6 Flow chart of the SLIM design procedure.

Step (c) The user interactive program also allows us to enter the required electromagnetic thrust from a single SLIM stator unit, F_s' , and the rated rotor velocity, V_r , which is the steady state velocity of the rotor plate. The desired values for these parameters are also as shown in Table 4-2.

Table 4-2 Desired values of some of the parameters of SLIM

PARAMETER	DESIRED VALUE
Number of phases, m	3
RMS Line-to-Line Voltage (V), V_{line}	480
Electrical Frequency (Hz), f	60
Number of poles, p	4
Number of slots per pole per phase, q_1	1
Operational Slip, S	5% or 10%
Stator width (m), W_s	3.14
Coil span, θ_p	180°
Thickness of Aluminum sheet, d (m)	0.003
Stator Current Density (A/mm^2), J_I	6
Target thrust (N), F_s'	8611 or 8177
Rated rotor velocity (m/s), V_r	15.5
Physical air-gap (m), g_m	0.01

Step (d) The synchronous velocity, V_s , can now be calculated using (3.1) as

$$V_s = \frac{V_r}{(1-S)}. \quad (4.1)$$

Step (e) The pole pitch τ can be calculated using (3.2) as

$$\tau = \frac{V_s}{2f} \quad (4.2)$$

The slot pitch, λ can be calculated using (3.25) or

$$\lambda = \frac{\tau}{mq_1} \quad (4.3)$$

The length of one stator unit L_s , is given by the equation

$$L_s = p\tau. \quad (4.4)$$

Step (f) At first, assume that the slot width w_s is equal to the tooth width w_t , which is equal to half of the slot pitch, λ .

$$w_s = w_t = \frac{\lambda}{2} \quad (4.5)$$

Step (g) To begin with, we set the number of turns per slot N_c , to one and increment it by one until we meet our thrust requirement in the later part of the program.

The number of turns per phase N_l , can be computed using (3.31) as

$$N_l = N_c pq_1 \quad (4.6)$$

Step (h) Initially, assign the product of $\eta \cos \phi$ between 0 and 1 to any arbitrary value, say 0.2. This value will be changed later in the program based on the calculated

value of $\eta\cos\phi$.

Step (i) The estimated rated stator RMS current can be found using equation (3.14) with F_s and I_l replaced with F_s' and I_l' respectively. Then,

$$I_1' = \frac{F_s' V_r}{m V_1 \eta \cos \phi} \quad (4.7)$$

where F_s' is the target thrust and V_r is the rotor velocity as shown in table 4-2, $\eta\cos\phi$ is the value from step (h), and V_1 is the rated line to neutral RMS primary voltage, which is given by

$$V_1 = \frac{V_{line}}{\sqrt{3}} \quad (4.8)$$

Step (j) Assuming, I_1' to be the rated stator current, the total cross sectional area of the copper wire, A_{wt} can be estimated using

$$A_{wt} = N_c A_w = \frac{I_1'}{J_1} \quad (4.9)$$

and the cross sectional area of the slot A_s can be (3.30) ,i.e.,

$$A_s = \frac{10}{7} N_c A_w \quad (4.10)$$

where J_1 is the specified stator current density from table 4-2. The stator slot height, h_s can be found using (3.29) where A_s is given by (4.10) in step (j).

Step (k) The magnetic air-gap, g_0 is calculated using (3.23), where d is the thickness of rotor outer conducting layer which is typically made of aluminum. Carter's coefficient, k_c is given by (3.24) where γ is computed using (3.26). Once the Carter's

coefficient is determined, we can compute the effective air-gap, g_e using (3.22). The Goodness factor is a measure of SLIM performance and is given by (3.44) as

$$G = \frac{2\mu_0 f \tau^2}{\pi \left(\frac{\rho_r}{d}\right) g_e} . \quad (4.11)$$

Step (l) The length of copper wire per phase can be calculated from (3.36) i.e,

$$l_w = N_l l_{wl} \quad (4.12)$$

where

$$l_{wl} = 2(W_s + l_{ce}), \quad (4.13)$$

is the mean length of one turn of the stator windings per phase and the total sum of stator width W_s and length of end connection coil l_{ce} is called effective stator width W_{se} . The pitch factor of the coil is given by (3.8) and the distribution factor k_d is given by (3.9). The product of pitch factor k_p and distribution factor k_d gives us the winding factor of the coil k_w .

Step (m) The equivalent circuit parameters of SLIM can be determined using the per-phase equivalent circuit as shown in Fig 3-5. The per-phase stator resistance, R_l can be determined using (3.35) where the length of copper wire per phase l_w is as given by (3.36) and the cross sectional area of the copper wire, A_w is given by (4.9) in step (j).

The per phase slot leakage reactance X_l can be determined using (3.37) and the per-phase magnetizing reactance X_m can be found using (3.41). The ratio of magnetizing reactance given by (3.41) and the goodness factor in (4.11) gives us the per phase rotor resistance R_2 , as in (3.43)

Step (n) Using the equivalent circuit parameters from step (m) and the equivalent circuit diagram as shown in Fig 3-5 in Chapter 3, the rated value of unit impedance* of the SLIM can be determined using the following equation

$$Z = R_1 + jX_1 + \frac{j\left(\frac{R_2}{S} X_m\right)}{\frac{R_2}{S} + jX_m} \quad (4.14)$$

$$Z = |Z| \angle \phi \quad (4.15)$$

where $|Z|$ is the magnitude of unit impedance*, ϕ is the phase angle of Z and S is the rated slip as given in Table 4-2. The power factor of the SLIM unit is given by the cosine of the phase angle of Z , $\cos\phi$. The actual SLIM stator RMS current can be determined by

$$I_1 = \frac{V_1}{|Z|} \quad (4.16)$$

where V_1 is the rated primary RMS voltage given by (4.6) and $|Z|$ by (4.14). The RMS value of the magnetizing current I_m can be given as follows.

$$I_m = \frac{I_1 R_2}{\sqrt{R_2^2 + (S X_m)^2}} \quad (4.17)$$

Step (o) At a desired value of rotor velocity, V_r , as specified in Table 4-2, the actual SLIM electromagnetic thrust can be calculated using (3.49), as shown in Chapter 3. The output power can be calculated with (3.47) and the input power with (3.51). The efficiency of the SLIM can thus be calculated using (3.52).

Step (p) The actual value of $\eta \cos\phi$ is then calculated and compared with the assumed value of $\eta \cos\phi$ in step (g). If the difference between the calculated and the

* Unit impedance refers to the impedance of one stator unit.

assumed value is not within a margin of 0.01%, we proceed to step (q), where we take the average of the assumed value and calculated value of $\eta \cos \phi$ and redo steps (i) through (p). This is one of the iteration loops in the program, which is repeated until the calculated value of $\eta \cos \phi$ is within 0.01% of the assumed value of the same.

Step (q) When the calculated value of $\eta \cos \phi$ is within 0.01% of its assumed value, we check whether the calculated value of actual SLIM thrust is equal to the target thrust specified in the beginning of the program in step (c). If they are not equal, we increment the number of turns per slot, N_c , and redo steps (g) through (q). This is a second iterative loop which will be executed until the calculated value is close to the target thrust which is done by bracketing the calculated value of thrust. Thus, there are two nested iterative loops in the program which will be executed until we obtain the most optimum values for $\eta \cos \phi$, N_c , and F_s .

Step (r) After finding the optimum values for $\eta \cos \phi$, N_c , and F_s , the size of copper wire for stator windings, the number of parallel wires N_p and their arrangement inside a stator slot can be determined. Since the stator current is very high, of the order of hundreds of amperes, we need a very thick wire of high cross sectional area to carry this current, which in turn makes it difficult to wind it across the slots. Hence, we divide this total current among a set of parallel wires which will now equally distribute the total current among themselves. This will reduce the cross sectional area of the individual copper wire and hence make it easy to wind. The copper wire gauge and the number of parallel wires must be properly selected based on tooth flux requirements, stator current

density, and the arrangements of these conductors inside the slots.

Step (s) Based on the specified value of the size of copper wire and the number of parallel wires which is initially set to 1, the values of slot width w_s , tooth width w_t and slot depth h_s are recalculated. In order to find the new value of slot width w_s , a slot insulation factor t_I of 1.1mm for 480V should be considered to provide ground fault insulation. The new value of slot width can be given as

$$w_s = D_w N_p + 2t_I \quad (4.18)$$

where D_w is the diameter of selected copper wire gauge and N_p is the number of parallel wires. The new value of tooth width w_t can be given as the difference of slot pitch λ and slot width determined using (4.18).

$$w_t = \lambda - w_s \quad (4.19)$$

The height of stator slot h_s is given by (3.25) where w_s is the new value given by (4.18).

Step (t) Based on the new values of the slot parameters found in step (s), Carter's coefficient k_c , effective air-gap g_e and the goodness factor G are recalculated using (3.24), (3.22) and (3.44) respectively.

Step (u) The equivalent circuit parameters R_1 , X_1 , X_m and R_2 are recalculated using the equations given in Chapter 3.

Step (v) There should be a minimum value for tooth width to produce the required flux density which is given by (3.28) in terms of B_{gavg} and B_{tmax} . The stator windings generate a magneto-motive force M which is given as

$$M = \frac{B_{g \max} \mathcal{G}_e}{\mu_0} \quad (4.20)$$

The SLIM magnetomotive force which is produced by all the stator windings of m phases is given as

$$M = \frac{2\sqrt{2}mk_w N_1 I_m}{\pi p} \quad (4.21)$$

By equating equations (4.20) and (4.21) and using (3.20) we get

$$B_{g \text{avg}} = \frac{4\sqrt{2}mk_w N_1 I_m \mu_0}{\pi^2 \mathcal{G}_e p} \quad (4.22)$$

The minimum tooth density given by (3.28) can be now written as

$$w_{t \min} = \frac{2\sqrt{2}mk_w N_1 I_m \mu_0 \lambda}{\pi \mathcal{G}_e p B_{t \max}} \quad (4.23)$$

If the value of minimum tooth width is greater than the tooth width, we change the number of parallel wires and their arrangement inside a slot, increment the number of parallel wires, and repeat steps (s) through (v) until the value of tooth width is greater than the minimum tooth width determined by (4.20).

Step (w) Update the value of estimated stator current I_1' and then calculate the value of stator current density J_1 using (4.9) as

$$J_1 = \frac{I_1'}{A_w} \quad (4.24)$$

Step (x) The yoke height of the stator core h_y is calculated using (3.33).

Step (y) At rated rotor velocity V_r , the final values of actual SLIM thrust F_s , SLIM

output power p_o , input power p_i , and efficiency η are calculated.

The difference between the actual SLIM thrust F_s and the target value F_s' is calculated and its value is stored in an array. Then we select the next wire gauge and repeat step (r) through step (y). This process is repeated for all the wire gauges available and the new value of the difference between actual SLIM thrust F_s and the target value F_s' is stored in the same array. The wire gauge which gives the minimum difference between F_s and F_s' and also satisfies all the above constraints is selected as the most suitable wire gauge for this design of the SLIM.

This is the complete procedure for the design of a single SLIM stator unit using a user interactive computer program, for which the flow chart is as shown in Fig 4-6. This program allows the user to choose a variety of desired values in the design of SLIM unit like the desired SLIM thrust, rotor velocity, rated slip and many other design parameters.

4.3. Amounts of materials required for the construction of one SLIM stator unit

The length of one turn of copper winding inside a stator slot is given by twice the sum of stator width W_s and length of end connection l_{ce} . From the fractional pitch, double layer configuration shown in fig 4-3, the length of N_l turns of copper winding inside a stator slot is given by,

$$l_w = 2(W_s + l_{ce})N_l \quad (4.25)$$

For a SLIM, having m phases and N_p number of parallel wires in the stator slots, the total

length of copper wire needed for the stator windings is given as

$$T_{lw} = m * N_p * l_w. \quad (4.26)$$

From the design procedure stated above, the number of parallel wires required for the design of a specific SLIM can be obtained and hence the total length of copper wire required for the stator windings can be determined using 4.26. Using the AWG Standard table as shown in Appendix A, the total weight of copper required for stator windings can be found.

The total amount of iron required for the construction of one stator unit is determined by the sum of iron required for the stator yoke and the iron required for the stator tooth. From the stator slot geometry shown in Fig 3-3, the volume of core yoke can be obtained as

$$V_{yoke} = L_s W_s h_y \quad (4.27)$$

where, L_s is the length of the stator, W_s is the width of the stator and h_y is the height of core yoke. The volume of one tooth can be obtained from the stator core geometry shown in Fig 3-3, as follows

$$V_{tooth} = W_s w_t h_s \quad (4.28)$$

where w_t is the tooth width and h_s is the height of the slot. The total volume of the teeth is given by the product of volume of one tooth given by 4.28 and the number of teeth for one section of SLIM stator. It can be expressed as,

$$V_{teeth} = (mpq_1) W_s w_t h_s \quad (4.29)$$

The total iron volume is given by the sum of volumes of teeth and yoke as shown below.

$$V_{iron} = W_s [L_s h_y + (mpq_1) h_s w_t] \quad (4.30)$$

The total iron weight is calculated as the product of density of iron and its volume from 4.30, which can be expressed as,

$$W_{iron} = \rho_{iron} V_{iron} \quad (4.31)$$

Finally, the total weight of one SLIM stator unit is the total sum of weights of copper and iron which can be expressed as follows

$$W_{stator} = W_{copper} + W_{iron} \quad (4.32)$$

where W_{copper} is the total weight of copper wire which can be obtained from the standard AWG tables.

Using the sequential procedure explained above, the SLIM is designed according to the desired values stated in table 4-2 and the results are tabulated from tables 4-4. The MATLAB program which generated these results is shown in Appendix B.

Before selecting the wire gauge, we determine the most suitable turns per slot, N_c , which will produce a thrust close to our target value, starting at a value of N_c equal to one. Let us consider the design in table 4-4. The criterion for selecting the correct number of turns per slot based on the difference between actual thrust and the target thrust is shown in table 4-3.

Table 4-3 Variation of actual thrust with number of turns per slot

Number of turns per slot, N_c	Actual thrust, F_s (N)	Difference, $F_s - F_s'$ (N)
1	82200	73589
2	20723	12112

3	8964	353
4	4834	-3777

It is evident that the difference between the actual thrust and the target thrust is minimum when turns per slot is three. So, based on these values, the next iteration is performed to select the most suitable wire gauge for a particular design. The same iterative procedure is carried for any other design parameters.

From table 4-4, it can be seen that at a slip of 10% and for a target thrust of 8611N, the closest possible value for the actual thrust developed is 8658N at an efficiency of 79.88%. This is achieved with a gauge 5 wire having 3 turns per slot, with each turn having 8 parallel wires. The slot width to tooth width ratio is much greater than 50%.

From the table 4-5, it is evident that at the same slip of 10% and for a target thrust of 8171N, the closest possible thrust is 8356N. Also, slot width is much greater than the tooth width. At a slip of 5%, for a target thrust of 8611N, the actual thrust developed is 10640N at an efficiency of 82.2% as shown in table 4-6. For a target thrust of 8171N and at a slip of 5%, the actual thrust developed by one stator unit of SLIM is 10628N as shown in table 4-7. This design uses a gauge 3 wire having 2 turns per slot, with each turn having 6 parallel wires.

Table 4-4 Design parameters of SLIM at 10% slip and target thrust of 8611N.

No.	Description	Symbol	Design 1	Design 2	Design 3
1	Slots per pole per phase	q_l	1	1	1
2	Yoke flux density (tesla)	B_{ymax}	1.3	1.3	1.3
3	Tooth flux density (tesla)	B_{tmax}	1.6	1.6	1.6
4	Core width (m)	W_s	3.1416	3.1416	3.1416
5	SLIM Synchronous velocity (m/s)	V_s	17.22	17.22	17.22
6	Rotor velocity (m/s)	V_r	15.5	15.5	15.5
7	No of poles	p	4	4	4
8	Pole pitch (m)	τ	0.1435	0.1435	0.1435
9	Slot pitch (m)	λ	0.0478	0.0478	0.0478
10	Stator length (m)	L_s	0.574	0.574	0.574
11	"Target" thrust (N)	F_s'	8611	8611	8611
12	Number of turns per slot	N_c	3	3	3
13	Number of turns per phase	N_l	12	12	12
14	Estimated thrust based on N_c	F_{Nc}	8964	8964	8964
15	Copper wire size in winding	-	#3	#4	#5
16	Diameter without insulation (mm)	D_w	5.826	5.189	4.62
17	Slot width (m)	w_s	0.0372	0.0385	0.0392
18	Tooth width (m)	w_t	0.0107	0.0093	0.0087
19	Minimum tooth width	w_{tmin}	0.0068	0.0069	0.0069
20	Slot depth (m)	h_s	0.0184	0.0165	0.0147
21	Stator core yoke height (m)	h_y	0.0160	0.0161	0.0162
22	Actual thrust at specified V_r (N)	F_s	8375	8519	8658
23	Output power at specified V_r (KW)	P_{out}	129.82	132.05	134.21
24	Input power at specified V_r (KW)	P_{in}	161.52	164.98	168.01
25	Stator efficiency at specified V_r (%)	η	80.37	80.04	79.88
26	Actual rated stator RMS current (A)	I_l	464.87	477.8	486.12
27	Parallel wires in one turn of winding	N_p	6	7	8
28	Actual stator current density (A/mm ²)	J_l	2.91	3.22	3.62
29	Area of slot (cm ²)	A_s	6.85	6.34	5.74
30	Total area of wire (cm ²)	A_{wt}	4.8	4.44	4.02
31	Total length of copper wire (m)	T_{lw}	1418.47	1654.8	1891.3
32	Total weight of copper wire (Kg)	W_{copper}	336.14	311.33	282.02
33	Weight of Iron core (Kg)	W_{iron}	286.93	275.4	269.2
34	Total weight of one SLIM stator (Kg)	W_{stator}	623.07	586.73	551.22

Table 4-5 Design parameters of SLIM at 10% slip and target thrust of 8171N.

<u>No.</u>	<u>Description</u>	<u>Symbol</u>	<u>Design 1</u>	<u>Design 2</u>
1	Slots per pole per phase	q_1	1	1
2	Yoke flux density (tesla)	$B_{y_{max}}$	1.3	1.3
3	Tooth flux density (tesla)	$B_{t_{max}}$	1.6	1.6
4	Core width (m)	W_s	3.1416	3.1416
5	SLIM Synchronous velocity (m/s)	V_s	17.22	17.22
6	Rotor velocity (m/s)	V_r	15.5	15.5
7	No of poles	p	4	4
8	Pole pitch (m)	τ	0.1435	0.1435
9	Slot pitch (m)	λ	0.0478	0.0478
10	Stator length (m)	L_s	0.574	0.574
11	"Target" thrust (N)	F_s	8171	8171
12	Number of turns per slot	N_c	3	3
13	Number of turns per phase	N_l	12	12
14	Estimated thrust based on N_c	F_{N_c}	9015	9015
15	Copper wire size in winding	-	#3	#4
16	Diameter without insulation (mm)	D_w	5.826	5.189
17	Slot width (m)	w_s	0.0372	0.0385
18	Tooth width (m)	w_t	0.0107	0.0093
19	Minimum tooth width	$w_{t_{min}}$	0.0068	0.0068
20	Slot depth (m)	h_s	0.0184	0.0165
21	Stator core yoke height (m)	h_y	0.0160	0.0161
22	Actual thrust at specified V_r (N)	F_s	8356	8499
23	Output power at specified V_r (KW)	P_{out}	129.5	131.74
24	Input power at specified V_r (KW)	P_{in}	162.2	165.71
25	Stator efficiency at specified V_r (%)	η	79.85	79.5
26	Actual rated stator RMS current (A)	I_l	464.34	484.16
27	Parallel wires in one turn of winding	N_p	6	7
28	Actual stator current density (A/mm^2)	J_l	2.9	3.22
29	Area of slot (cm^2)	A_s	6.85	6.3
30	Total area of wire (cm^2)	A_{wt}	4.8	4.44
31	Total length of copper wire (m)	T_{lw}	1418.47	1654.8
32	Total weight of copper wire (Kg)	W_{copper}	336.14	311.3
33	Weight of Iron core (Kg)	W_{iron}	286.93	275.4
34	Total weight of one SLIM stator (Kg)	W_{stator}	623.07	586.7

Table 4-6 Design parameters of SLIM at 5% slip and target thrust of 8611N.

No.	Description	Symbol	Design 1	Design 2	Design 3
1	Slots per pole per phase	q_l	1	1	1
2	Yoke flux density (tesla)	B_{ymax}	1.3	1.3	1.3
3	Tooth flux density (tesla)	B_{tmax}	1.6	1.6	1.6
4	Core width (m)	W_s	3.1416	3.1416	3.1416
5	SLIM Synchronous velocity (m/s)	V_s	16.31	16.31	16.31
6	Rotor velocity (m/s)	V_r	15.5	15.5	15.5
7	No of poles	p	4	4	4
8	Pole pitch (m)	τ	0.1360	0.1360	0.1360
9	Slot pitch (m)	λ	0.0453	0.0453	0.0453
10	Stator length (m)	L_s	0.544	0.544	0.544
11	"Target" thrust (N)	F_s'	8611	8611	8611
12	Number of turns per slot	N_c	2	2	2
13	Number of turns per phase	N_l	8	8	8
14	Estimated thrust based on N_c	F_{Nc}	9591	9591	9591
15	Copper wire size in winding	-	#3	#4	#5
16	Diameter without insulation (mm)	D_w	5.826	5.189	4.62
17	Slot width (m)	w_s	0.0372	0.0333	0.0345
18	Tooth width (m)	w_t	0.0107	0.0145	0.0133
19	Minimum tooth width	w_{tmin}	0.0108	0.0109	0.011
20	Slot depth (m)	h_s	0.0123	0.0109	0.0097
21	Stator core yoke height (m)	h_y	0.0254	0.0257	0.0258
22	Actual thrust at specified V_r (N)	F_s	10640	10853	10971
23	Output power at specified V_r (KW)	P_{out}	174.06	177.55	179.48
24	Input power at specified V_r (KW)	P_{in}	211.74	212.79	216.04
25	Stator efficiency at specified V_r (%)	η	82.2	83.44	83.08
26	Actual rated stator RMS current (A)	I_l	1004.2	956.15	978.57
27	Parallel wires in one turn of winding	N_p	6	6	7
28	Actual stator current density (A/mm ²)	J_l	6.227	7.53	8.34
29	Area of slot (cm ²)	A_s	3.8	3.62	3.35
30	Total area of wire (cm ²)	A_{wt}	2.66	2.54	2.34
31	Total length of copper wire (m)	T_{lw}	945.65	945.65	1103.26
32	Total weight of copper wire (Kg)	W_{copper}	224.1	177.91	165.52
33	Weight of Iron core (Kg)	W_{iron}	401.55	413.7	406.5
34	Total weight of one SLIM stator (Kg)	W_{stator}	625.65	591.61	572.02

Table 4-7 Design parameters of SLIM at 5% slip and target thrust of 8171N.

No.	Description	Symbol	Design 1	Design 2	Design 3
1	Slots per pole per phase	q_l	1	1	1
2	Yoke flux density (tesla)	B_{ymax}	1.3	1.3	1.3
3	Tooth flux density (tesla)	B_{tmax}	1.6	1.6	1.6
4	Core width (m)	W_s	3.1416	3.1416	3.1416
5	SLIM Synchronous velocity (m/s)	V_s	16.31	16.31	16.31
6	Rotor velocity (m/s)	V_r	15.5	15.5	15.5
7	No of poles	p	4	4	4
8	Pole pitch (m)	τ	0.1360	0.1360	0.1360
9	Slot pitch (m)	λ	0.0453	0.0453	0.0453
10	Stator length (m)	L_s	0.544	0.544	0.544
11	"Target" thrust (N)	F_s'	8171	8171	8171
12	Number of turns per slot	N_c	2	2	2
13	Number of turns per phase	N_l	8	8	8
14	Estimated thrust based on N_c	F_{Nc}	9699	9699	9699
15	Copper wire size in winding	-	#3	#4	#5
16	Diameter without insulation (mm)	D_w	5.826	5.189	4.62
17	Slot width (m)	w_s	0.0372	0.0333	0.0345
18	Tooth width (m)	w_t	0.0107	0.0145	0.0133
19	Minimum tooth width	w_{tmin}	0.0108	0.0109	0.011
20	Slot depth (m)	h_s	0.0123	0.0109	0.0097
21	Stator core yoke height (m)	h_y	0.0254	0.0257	0.0258
22	Actual thrust at specified V_r (N)	F_s	10628	10842	10959
23	Output power at specified V_r (KW)	P_{out}	173.87	177.36	179.28
24	Input power at specified V_r (KW)	P_{in}	213.28	214.16	217.48
25	Stator efficiency at specified V_r (%)	η	81.52	82.81	82.44
26	Actual rated stator RMS current (A)	I_l	1003.6	955.63	978.64
27	Parallel wires in one turn of winding	N_p	6	6	7
28	Actual stator current density (A/mm ²)	J_l	6.27	7.53	8.33
29	Area of slot (cm ²)	A_s	3.8	3.62	3.35
30	Total area of wire (cm ²)	A_{wt}	2.66	2.54	2.34
31	Total length of copper wire (m)	T_{tw}	945.65	945.65	1103.26
32	Total weight of copper wire (Kg)	W_{copper}	224.1	177.91	164.52
33	Weight of Iron core (Kg)	W_{iron}	401.55	413.71	406.48
34	Total weight of one SLIM stator (Kg)	W_{stator}	625.65	591.62	571

From the above results, it is evident that the slot width is much greater than the tooth width. Also, the actual thrust developed by SLIM is not very close to the target thrust as desired. Improvements to the above designs are done by making the ratio of slot width to tooth width close to 50%. This is achieved by specifying a greater margin for the difference between the tooth width and the minimum tooth width. The improved results are as shown in tables 4-8, 4-9, 4-10 and 4-11.

From table 4-8, it can be seen that the stator width is almost equal to the tooth width making the ratio close to 50%. For a SLIM having a target thrust of 8611N and operating at a slip of 10%, the closest value of actual thrust possible is 8610N. This is achieved using a gauge 6 wire having 3 turns per slot with each turn having 5 parallel wires. The efficiency is as high as 82.62% compared to 79.88% in table 4-4. When the target thrust is 8171N and at the same slip of 10%, the actual thrust developed by the SLIM is 8161N at an efficiency of 81.9% compared to the design from table 4-5 where the actual thrust is 8356N at an efficiency of 79.85%.

The modified design of the SLIM at a slip of 5% for a target thrust of 8611N and 8171N are shown in tables 4-10 and 4-11 respectively. These designs have a better ratio of slot width to tooth width compared to the previous results. Hence, the final thrust obtained from these designs is much closer to the target thrust at a better efficiency.

Table 4-8 Design parameters of SLIM at 10% slip and target thrust of 8611N.

No.	Description	Symbol	Design 1	Design 2	Design 3
1	Slots per pole per phase	q_l	1	1	1
2	Yoke flux density (tesla)	B_{ymax}	1.3	1.3	1.3
3	Tooth flux density (tesla)	B_{tmax}	1.6	1.6	1.6
4	Core width (m)	W_s	3.1416	3.1416	3.1416
5	SLIM Synchronous velocity (m/s)	V_s	17.22	17.22	17.22
6	Rotor velocity (m/s)	V_r	15.5	15.5	15.5
7	No of poles	p	4	4	4
8	Pole pitch (m)	τ	0.1435	0.1435	0.1435
9	Slot pitch (m)	λ	0.0478	0.0478	0.0478
10	Stator length (m)	L_s	0.574	0.574	0.574
11	"Target" thrust (N)	F_s	8611	8611	8611
12	Number of turns per slot	N_c	3	3	3
13	Number of turns per phase	N_l	12	12	12
14	Estimated thrust based on N_c	F_{Nc}	8964	8964	8964
15	Copper wire size in winding	-	#5	#6	#7
16	Diameter without insulation (mm)	D_w	4.62	4.1148	3.6652
17	Slot width (m)	w_s	.0253	.0228	.0242
18	Tooth width (m)	w_t	.0225	.0251	.0236
19	Minimum tooth width	w_{tmin}	.0069	.0069	.007
20	Slot depth (m)	h_s	.0142	.0125	.0112
21	Stator core yoke height (m)	h_y	.0162	.0162	.0164
22	Actual thrust at specified V_r (N)	F_s	8570	8610	8856
23	Output power at specified V_r (KW)	P_{out}	132.8	133.45	137.27
24	Input power at specified V_r (KW)	P_{in}	161.3	161.54	166.45
25	Stator efficiency at specified V_r (%)	η	82.34	82.62	82.47
26	Actual rated stator RMS current (A)	I_l	414.26	407.13	417.37
27	Parallel wires in one turn of winding	N_p	5	5	6
28	Actual stator current density (A/mm ²)	J_l	4.94	6.12	6.59
29	Area of slot (cm ²)	A_s	3.59	2.85	2.71
30	Total Area of wire (cm ²)	A_{wt}	2.514	1.992	1.896
31	Total length of copper wire (m)	T_{lw}	1182.06	1182.06	1418.5
32	Total weight of copper wire (Kg)	W_{copper}	176.21	139.84	133.02
33	Weight of Iron core (Kg)	W_{iron}	326.35	324.63	312.75
34	Total weight of one SLIM stator (Kg)	W_{stator}	502.56	464.47	445.77

* Best design of SLIM at 10% slip and target thrust of 8611N.

Table 4-9 Design parameters of SLIM at 10% slip and target thrust of 8171N.

No.	Description	Symbol	Design 1*	Design 2
1	Slots per pole per phase	q_l	1	1
2	Yoke flux density (Tesla)	$B_{y_{max}}$	1.3	1.3
3	Tooth flux density (Tesla)	$B_{t_{max}}$	1.6	1.6
4	Core width (m)	W_s	3.1416	3.1416
5	SLIM Synchronous velocity (m/s)	V_s	17.22	17.22
6	Rotor velocity (m/s)	V_r	15.5	15.5
7	No of poles	p	4	4
8	Pole pitch (m)	τ	0.1435	0.1435
9	Slot pitch (m)	λ	0.0478	0.0478
10	Stator length (m)	L_s	0.574	0.574
11	"Target" thrust (N)	F_s'	8171	8171
12	Number of turns per slot	N_c	3	3
13	Number of turns per phase	N_l	12	12
14	Estimated thrust based on N_c	F_{N_c}	9015	9015
15	Copper wire size in winding	-	#3	#4
16	Diameter without insulation (mm)	D_w	5.826	5.189
17	Slot width (m)	w_s	0.0255	0.023
18	Tooth width (m)	w_t	0.0223	0.0249
19	Minimum tooth width	w_{min}	0.0067	0.0067
20	Slot depth (m)	h_s	0.0179	0.0158
21	Stator core yoke height (m)	h_y	0.0158	0.0158
22	Actual thrust at specified V_r (N)	F_s	8161	8217
23	Output power at specified V_r (KW)	P_{out}	126.5	127.36
24	Input power at specified V_r (KW)	P_{in}	154.44	155
25	Stator efficiency at specified V_r (%)	η	81.9	82.18
26	Actual rated stator RMS current (A)	I_l	404.96	398.3
27	Parallel wires in one turn of winding	N_p	4	4
28	Actual stator current density (A/mm ²)	J_l	3.8	4.71
29	Area of slot (cm ²)	A_s	4.57	3.62
30	Total area of wire (cm ²)	A_{wt}	3.18	2.538
31	Total length of copper wire (m)	T_{lw}	945.648	945.648
32	Total weight of copper wire (Kg)	W_{copper}	224.1	177.91
33	Weight of Iron core (Kg)	W_{iron}	109.62	109.1
34	Total weight of one SLIM stator (Kg)	W_{stator}	333.7	287.01

* Best design of SLIM at 10% slip and target thrust of 8171N

Table 4-10 Design parameters of SLIM at 5% slip and target thrust of 8611N.

No.	Description	Symbol	Design 1*	Design 2	Design 3
1	Slots per pole per phase	q_l	1	1	1
2	Yoke flux density (tesla)	B_{ymax}	1.3	1.3	1.3
3	Tooth flux density (tesla)	B_{tmax}	1.6	1.6	1.6
4	Core width (m)	W_s	3.1416	3.1416	3.1416
5	SLIM Synchronous velocity (m/s)	V_s	16.31	16.31	16.31
6	Rotor velocity (m/s)	V_r	15.5	15.5	15.5
7	No of poles	p	4	4	4
8	Pole pitch (m)	τ	0.1360	0.1360	0.1360
9	Slot pitch (m)	λ	0.0453	0.0453	0.0453
10	Stator length (m)	L_s	0.544	0.544	0.544
11	"Target" thrust (N)	F_s	8611	8611	8611
12	Number of turns per slot	N_c	2	2	2
13	Number of turns per phase	N_l	8	8	8
14	Estimated thrust based on N_c	F_{Nc}	9591	9591	9591
15	Copper wire size in winding	-	#3	#4	#5
16	Diameter without insulation (mm)	D_w	5.826	5.189	4.62
17	Slot width (m)	w_s	.0197	.0178	.0161
18	Tooth width (m)	w_t	.0256	.0276	.0293
19	Minimum tooth width	w_{tmin}	.0103	.0103	.0103
20	Slot depth (m)	h_s	.0116	.0102	.0089
21	Stator core yoke height (m)	h_y	.0243	.0243	.0243
22	Actual thrust at specified V_r (N)	F_s	9658	9667	9659
23	Output power at specified V_r (KW)	P_{out}	149.72	149.8	149.7
24	Input power at specified V_r (KW)	P_{in}	175.61	175.16	174.5
25	Stator efficiency at specified V_r (%)	η	85.26	85.55	85.77
26	Actual rated stator RMS current (A)	I_l	810.89	797.84	7786.81
27	Parallel wires in one turn of winding	N_p	3	3	3
28	Actual stator current density (A/mm ²)	J_l	10.14	12.57	15.64
29	Area of slot (cm ²)	A_s	2.285	1.813	1.437
30	Total area of wire (cm ²)	A_{wt}	1.599	1.268	1.006
31	Total length of copper wire (m)	T_{lw}	471.97	471.97	471.97
32	Total weight of copper wire (Kg)	W_{copper}	111.85	88.8	70.36
33	Weight of Iron core (Kg)	W_{iron}	417.05	412.44	406.26
34	Total weight of one SLIM stator (Kg)	W_{stator}	528.9	501.24	476.62

* Best design of SLIM at 5% slip and target thrust of 8611N.

Table 4-11 Design parameters of SLIM at 5% slip and target thrust of 8171N.

No.	Description	Symbol	Design 1*	Design 2	Design 3
1	Slots per pole per phase	q_l	1	1	1
2	Yoke flux density (tesla)	$B_{y_{max}}$	1.3	1.3	1.3
3	Tooth flux density (tesla)	$B_{t_{max}}$	1.6	1.6	1.6
4	Core width (m)	W_s	3.1416	3.1416	3.1416
5	SLIM Synchronous velocity (m/s)	V_s	16.31	16.31	16.31
6	Rotor velocity (m/s)	V_r	15.5	15.5	15.5
7	No of poles	p	4	4	4
8	Pole pitch (m)	τ	0.1360	0.1360	0.1360
9	Slot pitch (m)	λ	0.0453	0.0453	0.0453
10	Stator length (m)	L_s	0.544	0.544	0.544
11	"Target" thrust (N)	F_s'	8171	8171	8171
12	Number of turns per slot	N_c	2	2	2
13	Number of turns per phase	N_l	8	8	8
14	Estimated thrust based on N_c	F_{N_c}	9699	9699	9699
15	Copper wire size in winding	-	#3	#4	#5
16	Diameter without insulation (mm)	D_w	5.826	5.189	4.62
17	Slot width (m)	w_s	.0197	.023	.0207
18	Tooth width (m)	w_t	.0256	.0224	.0246
19	Minimum tooth width	w_{tmin}	.0103	.0105	.0106
20	Slot depth (m)	h_s	.0116	.0105	.0093
21	Stator core yoke height (m)	h_y	.0242	.0248	.0248
22	Actual thrust at specified V_r (N)	F_s	9651	10089	10112
23	Output power at specified V_r (KW)	P_{out}	149.6	156.38	156.73
24	Input power at specified V_r (KW)	P_{in}	176.6	185.96	185.42
25	Stator efficiency at specified V_r (%)	η	84.7	84.09	84.53
26	Actual rated stator RMS current (A)	I_l	810.53	855.98	837.47
27	Parallel wires in one turn of winding	N_p	3	4	4
28	Actual stator current density (A/mm ²)	J_l	10.13	10.11	12.49
29	Area of slot (cm ²)	A_s	2.285	2.417	1.916
30	Total area of wire (cm ²)	A_{wt}	1.6	1.692	1.34
31	Total length of copper wire (m)	T_{tw}	471.97	629.3	629.3
32	Total weight of copper wire (Kg)	W_{copper}	111.85	118.4	93.81
33	Weight of Iron core (Kg)	W_{iron}	415.7	405.4	403.48
34	Total weight of one SLIM stator (Kg)	W_{stator}	527.55	523.8	497.3

* Best design of SLIM at 5% slip and target thrust of 8171N.

CHAPTER 5

PERFORMANCE CURVES AND DISCUSSION OF RESULTS

The user interactive design procedure of the SLIM is discussed in detail in the previous chapter and the results thus obtained are tabulated. In this Chapter, the performance curves of the SLIM are drawn and then analyzed for different target thrust values and rated slip. The effect of varying parameters of the SLIM such as air-gap, thickness of aluminum sheet and the number of poles on the performance of SLIM are then analyzed and the results are discussed. The results of design of the SLIM are then compared with a similar TLIM of the same desired performance values and the results are tabulated as shown in table 5-4.

5.1. Characteristic curves of SLIM

The SLIM designs for a rated rotor velocity of 15.5 m/s, a target thrust of 8611N and 8171 N, at rated slips of 5% and 10% are tabulated in tables 4-4, 4-5, 4-6, 4-7, 4-8, 4-9, 4-10 and 4-11. Once the design parameters were obtained, the performance of the SLIM stator as a function of rotor velocity, are evaluated as shown in the following figures. The performance curves of the SLIM, thrust F_s and efficiency η as a function of rotor velocity V_r , at a rated slip of 5% and a target thrust of 8611N are as shown in Fig 5.1 and Fig 5.2 using the results from table 4-10. The best design of the SLIM at a rated

slip of 10% and a desired speed of 8611N is shown in table 4-8. Using these results, the variation of thrust F_s and efficiency η with respect to rotor velocity V_r are shown in Fig 5-3 and Fig 5-4 respectively.

In order to sketch the characteristic curves of the SLIM, the following procedure is followed. The slip is varied from 0 to 1 in increments of 0.0001 and the unit impedance of the stator is calculated as a function of slip using

$$Z = R_1 + jX_1 + \frac{j\left(\frac{R_2}{S} X_m\right)}{\frac{R_2}{S} + jX_m} \quad (5.1)$$

$$Z = |Z|\angle\phi \quad (5.2)$$

where $|Z|$ is the magnitude of unit impedance. The actual SLIM stator RMS current is then calculated using

$$I_1 = \frac{V_1}{|Z|} \quad (5.3)$$

The resulting thrust is then calculated using (3.51) as

$$F_s = \frac{mI_1^2 R_2}{\left[\frac{1}{(SG)^2} + 1\right] V_s S} \quad (5.4)$$

The output power is calculated using (3.49) and the input power using the equation (3.53). The efficiency is thus calculated using equation (3.54) for different values of thrust. At a particular synchronous velocity V_s , the rated rotor velocity V_r is calculated at different slips from 0 to 1 using the equation (3.1). The performance curves, thrust and efficiency are then plotted versus varying rotor speed V_r as shown below.

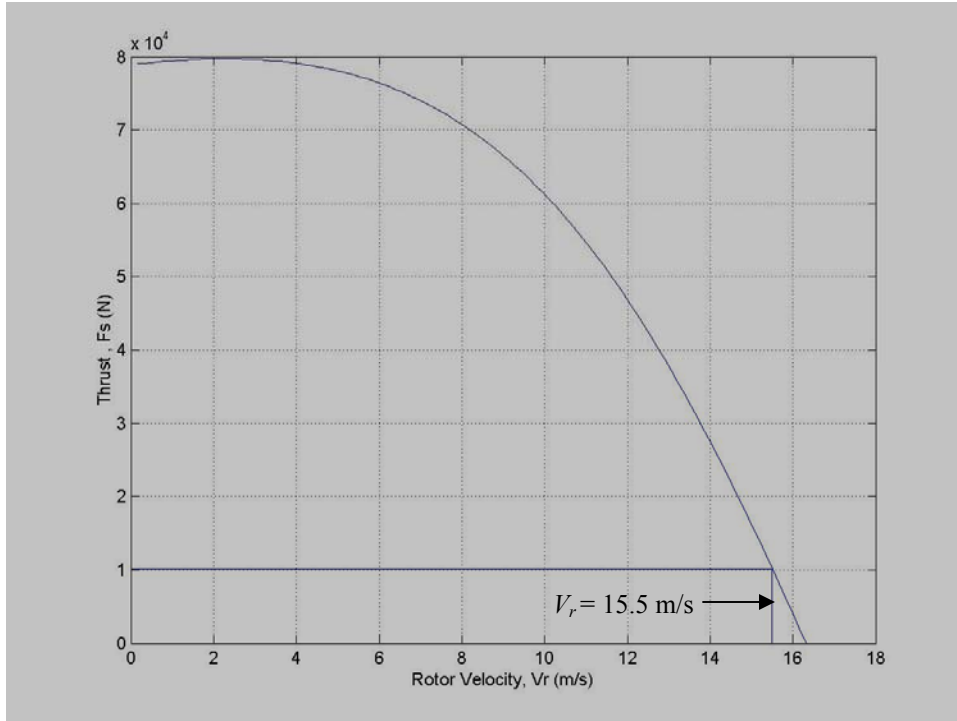


Fig 5.1 Thrust F_s versus rotor velocity V_r of one SLIM stator unit at a rated slip of 5%, a desired rotor velocity of 15.5 m/s, a target thrust of 8611N and final thrust of 9658N

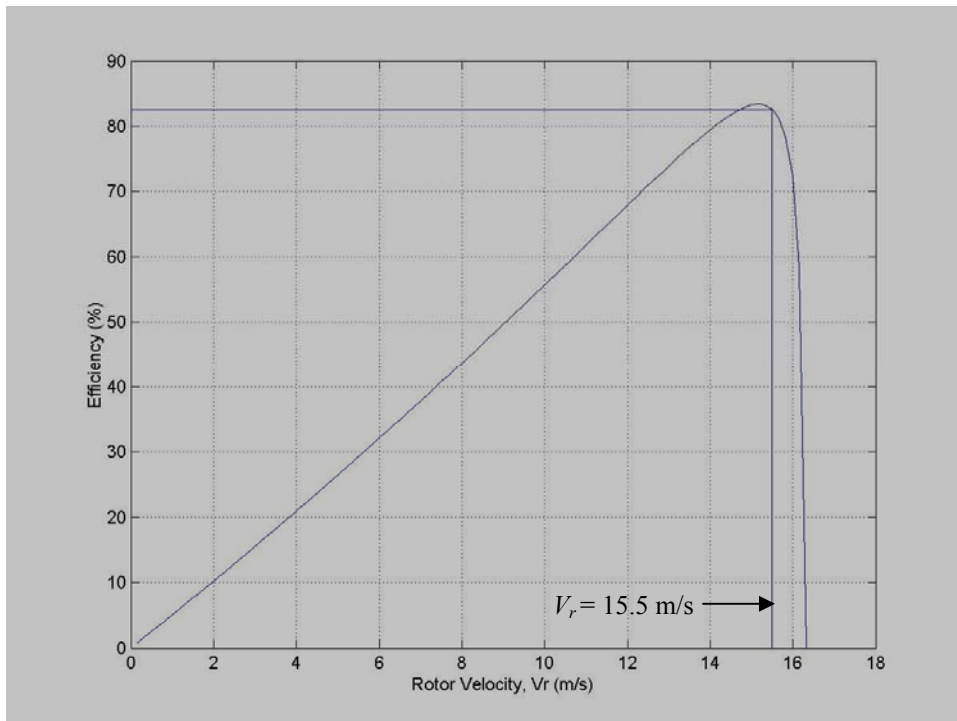


Fig 5.2 Efficiency η versus rotor velocity V_r of one SLIM stator unit at a rated slip of 5%, a desired rotor velocity of 15.5 m/s and target thrust of 8611N.

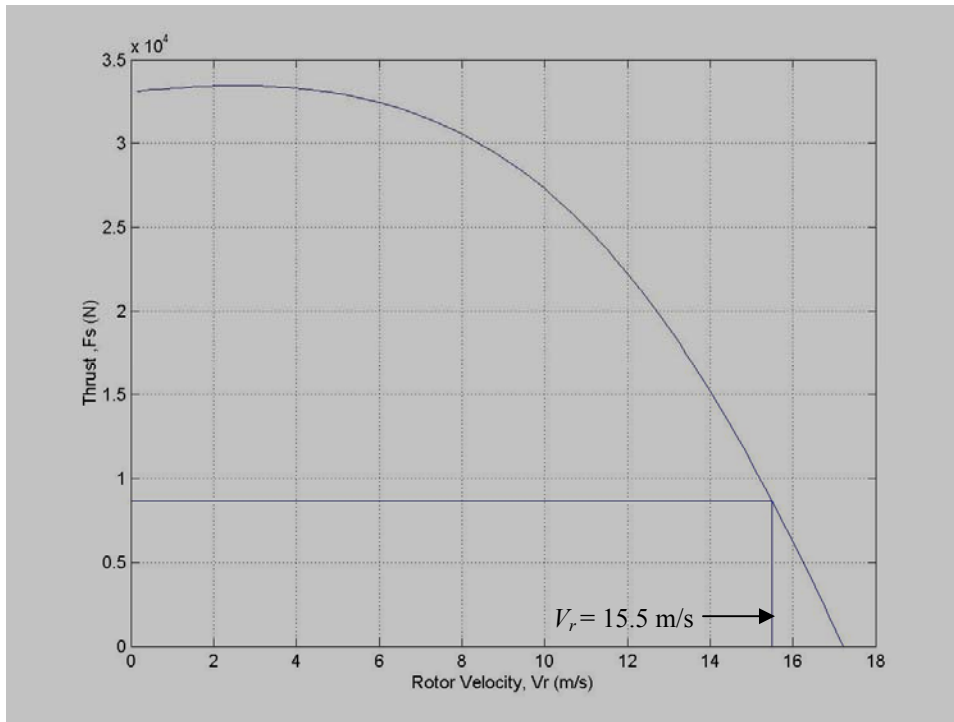


Fig 5.3 Thrust F_s versus rotor velocity V_r of one SLIM stator unit at a rated slip of 10%, a desired rotor velocity of 15.5 m/s, a target thrust of 8611N and a final thrust of 8610N.

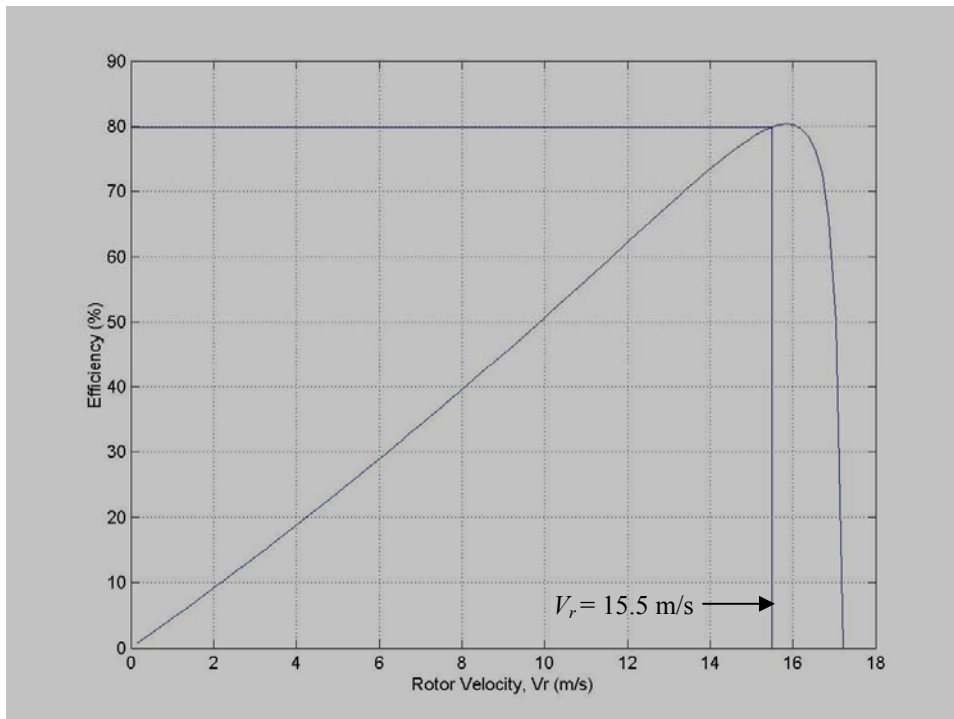


Fig 5.4 Efficiency η versus rotor velocity V_r of one SLIM stator unit at a rated slip of 10%, a desired rotor velocity of 15.5 m/s and target thrust of 8611N.

5.2. Evaluation of performance of SLIM by changing parameters

From the various designs of the SLIM at a rated slip of 10% and a target thrust of 8611N as shown in Chapter 4, we choose design 2 in table 4-8 as the best design of the SLIM. The performance of the SLIM based on this particular design is evaluated by varying certain parameters like the thickness of secondary, mechanical air-gap and the number of poles. Based on this evaluation, the best possible values for these parameters are selected as shown in the sections below.

5.2.1. Effect of Aluminum thickness on the performance parameters

The effect of varying the thickness of the aluminum sheet on the rotor of SLIM on its performance, from 1mm to 5mm in steps of 1mm is as shown in Fig 5-5 and Fig 5-6. The goodness factor of a SLIM is given by equation 3.46, where the thickness of aluminum sheet on the rotor, d , plays a significant role in the performance. From equation 3.46, it can be seen that, the thicker the secondary, the larger the goodness factor. Also, thicker aluminum sheet will increase the magnetic air-gap, as given by equation 3.19, which is undesirable. For nonferrous secondaries, the thickness must be small but large enough to withstand the forces present on the rotor. The performance parameters thrust and efficiency of SLIM, at various thickness of aluminum sheet at rated rotor velocity, can be tabulated as given in table 5-1.

Table 5-1 Aluminum sheet thickness effects on thrust and efficiency at rated rotor speed

Aluminum Thickness (mm)	Thrust (N)	Efficiency (%)
1	7529	82.52
2	6142	83.59
3	8610	82.62
4	5918	83.43
5	6900	82.74

As the thickness of Aluminum sheet is increased the magnitude of thrust also increases. But, as stated before, as the thickness of secondary sheet is increased the magnetic air-gap also increases which causes the magnitude of thrust to decrease, which can be seen in table 5-1. The efficiency does not have significant impact with an increase in aluminum thickness. It can be seen that various aluminum thicknesses have the same efficiency at the rated rotor velocity.

From Fig 5-5 and 5-6, it can be seen that the magnitude of thrust at rated velocity is maximum when the thickness of aluminum is 3mm at a reasonable value of efficiency. The actual thrust developed is 8610N at an efficiency of 82.6% for the SLIM operating at 10% slip and target thrust of 8611N as shown in table 4-8. Hence, a value of 3mm is chosen as the best value which yields maximum thrust at a reasonable efficiency.

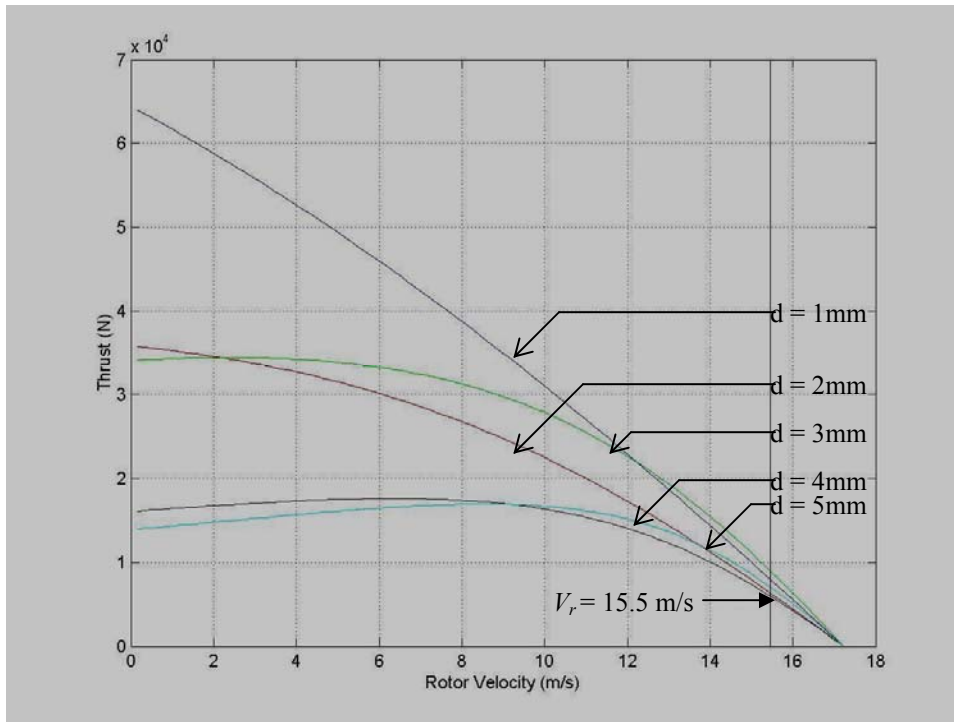


Fig 5-5 Effect of aluminum thickness on the thrust of SLIM plotted against rotor velocity at a rated slip of 10%, a desired rotor velocity of 15.5 m/s and target thrust of 8611N.

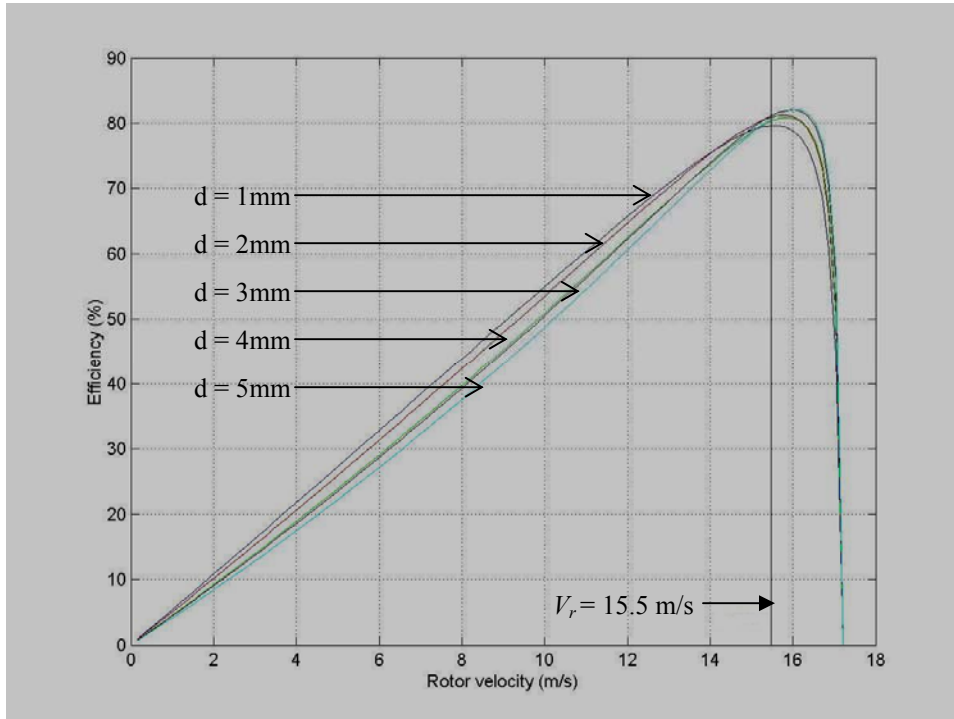


Fig 5-6 Effect of varying Aluminum thickness on efficiency of SLIM plotted against rotor velocity at a rated slip of 10%, a desired rotor velocity of 15.5 m/s and target thrust of 8611N.

As the thickness is increased beyond a certain value, the magnetic air-gap increases, which will reduce the flux linkage between the currents produced in the stator and the rotor conductor. Hence, an optimum value must be chosen for the thickness of the secondary conductor, which is 3mm for this particular design.

5.2.2. Effect of Mechanical air-gap on performance:

The different performance values with varying air-gap for the design 2 shown above are shown in table 5-2. When the air-gap is changed from 0.5 cm to 5 cm, keeping all other parameters fixed, the efficiency decreases with increasing air-gap, as shown in 5-8. As the air-gap is increased, the stand-still thrust or the thrust when the rotor is stationary, decreases except for 3cm case where the stand-still thrust is maximum. The stand still thrust decreases as the air-gap is increased from 0.5 to 2 cm. It can be also seen that at an air-gap of 3cm, there is a sudden increase in thrust which decreases at higher values of 4 and 5cm. The efficiency of SLIM also decreases with increase in air-gap. The efficiency reaches its peak at a rotor velocity close to its synchronous velocity of 17.22 m/s.

Table 5-2 Air-gap effects on thrust and efficiency

Air-gap (cm)	Thrust (N)	Efficiency (%)
0.5	10244	83.63
1	8610	82.62
2	6253	81.04
3	10442	76.40

4	7729	77.17
5	6954	77.65

The length of the air-gap is a very important parameter in machine design. A large air-gap requires a large magnetizing current and results in a smaller power factor. In the case of an LIM, the exit-end area losses increase with a large air-gap. Also, output force and efficiency are decreased when the design incorporates a large air-gap. As the equation 3.46 suggests, goodness factor is inversely proportional to the air-gap. For a low-speed LIM, the larger the goodness factor, the better the machine. Thus, it is clear that the air-gap should be as small as is mechanically possible [1].

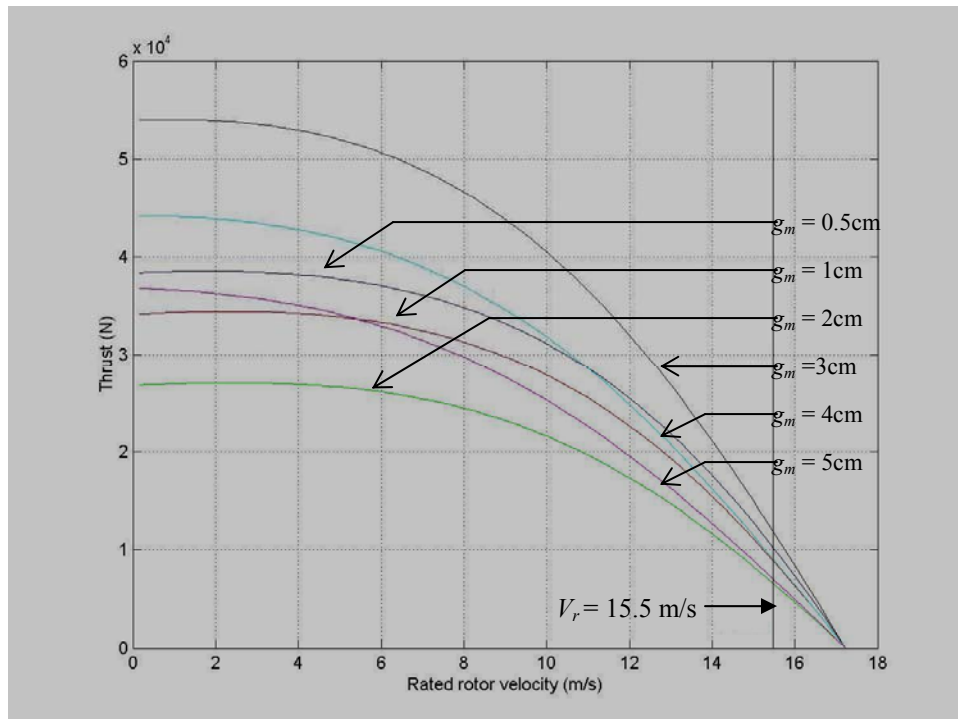


Fig 5-7 Effect of mechanical air-gap on thrust of SLIM at a rated slip of 10% and a target thrust of 8611 N for the design 2 in table 4-8.

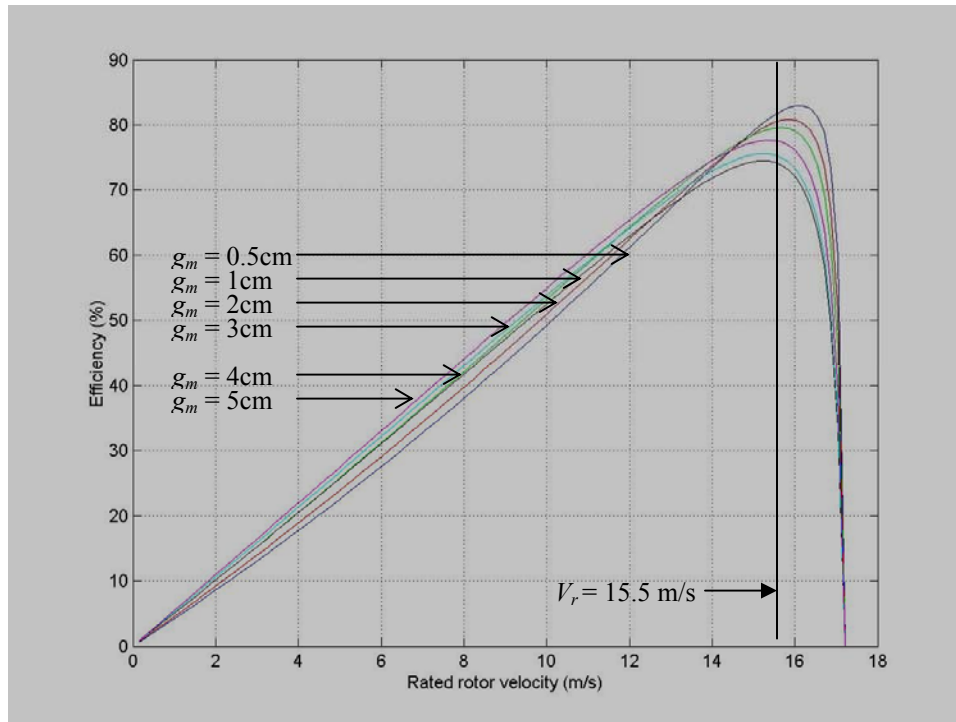


Fig 5-8 Effect of mechanical air-gap on efficiency of SLIM at a rated slip of 10% and a target thrust of 8611 N for the design 2 in table 4-8.

From above characteristic curves, it can be seen that available thrust close to the target thrust is possible when the air-gap is 1cm at a decent efficiency. Thus, a physical air-gap of 1cm is considered in the design of SLIM.

5.2.3 Effect of changing number of poles on Performance

When the number of poles is increased, the end effects are reduced in a LIM. This is because the end-effect loss is shared by a large number of poles, resulting in a better performing machine. Thus, it is advantageous to have a machine with a large number of poles. From equation 3.2, for a given synchronous speed and given frequency, the LIM may be very long unless a compromise in the number of poles is made.

The characteristic curves with respect to changing poles are as shown in fig 5-9

and 5-10. The standstill thrust increases as we increase the number of poles. Also, from fig 5-10 we can see that the efficiency decreases with increase in number of poles. Hence, there is trade off between the thrust and the efficiency with increasing number of poles. Also, there is a constraint on the length of the motor, which increases with the increase in number of poles when the synchronous velocity and supply frequency are assumed to be constant. Table 5-3 shows the effect of increasing number of poles on performance and also on the length of the motor.

Table 5-3 Effect of changing number of poles on the performance

No. of poles	Length of stator (m)	Thrust (N)	Efficiency (%)
2	0.2870	8368	84.74
4	0.5740	8610	82.62
8	1.148	10474	78.55

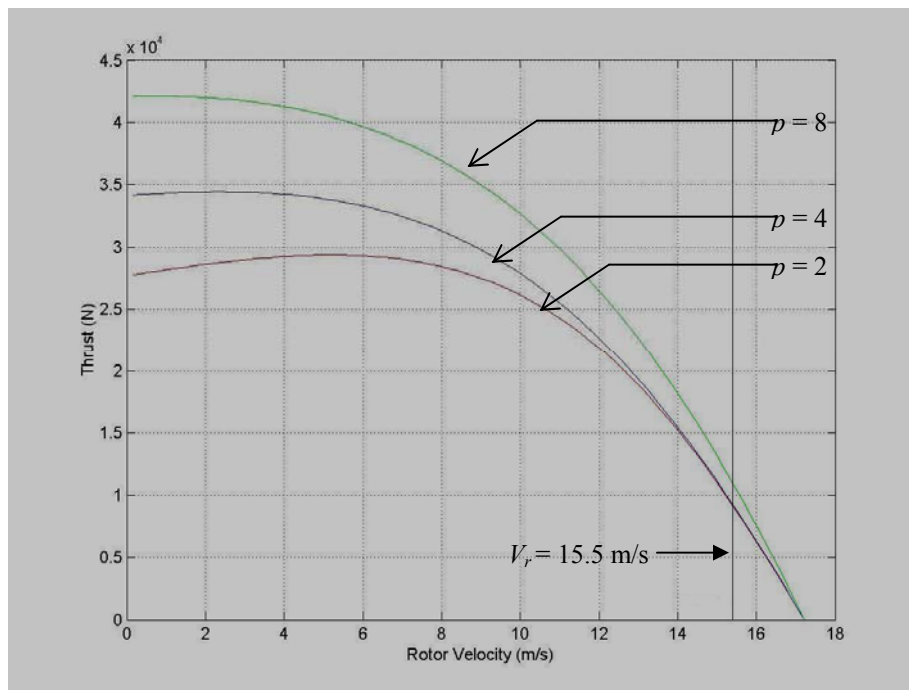


Fig 5-9 Effect of changing poles on the thrust developed by a SLIM versus rated rotor velocity for the design 2 in table 4-8.

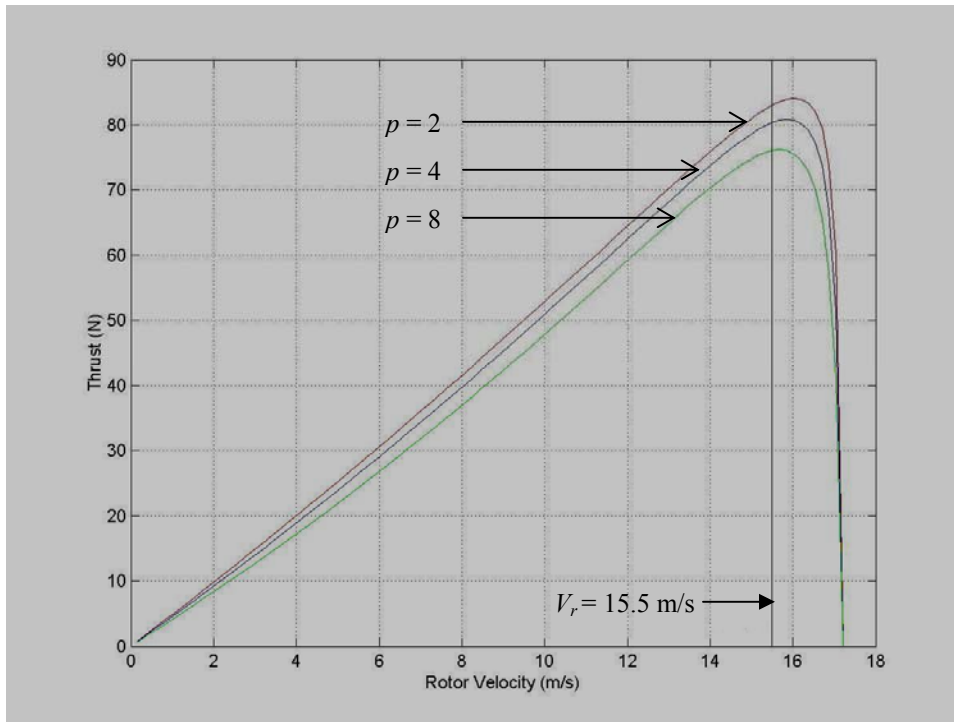


Fig 5-10 Effect of changing poles on the efficiency of a SLIM plotted against rated rotor velocity for the design 2 in table 4-8.

5.3. Comparing the results of the SLIM and the TLIM of same desired values

The design and analysis of the TLIM was studied by Plodpradista[29]. The results obtained from the design of the SLIM from Chapter 4 are compared with the design of the TLIM for the same desired values. Two models of TLIM and SLIM, 10% slip at a target thrust of 8611N and 5% slip at a target value of 8171N are compared as shown in table 5-4.

For an operating slip of 10% and a target thrust of 8611N, the actual thrust developed by the TLIM is 7357N which is 1254N less than the target value. For the same design of the SLIM, the actual thrust developed is 8610N which is almost equal to the target value. This is achieved by modifying the design algorithm of the SLIM and making the ratio of slot width to tooth width closely equal to 50%. The efficiencies of both TLIM

and the SLIM are comparable. It can be seen that this design of the SLIM could get close to the desired value meeting all the constraints involved in the design algorithm which were discussed in Chapter 4.

Table 5-4 Comparison of the TLIM and the SLIM of same desired values

		TLIM1	SLIM1	TLIM2	SLIM2
1	Rated Slip S	0.1	0.1	0.05	0.05
2	Yoke density $B_{y_{max}}$ (tesla)	1.3	1.3	1.3	1.3
3	Tooth density $B_{t_{max}}$ (tesla)	1.6	1.6	1.6	1.6
4	Core width W_s (m)	3.1416	3.1416	3.1416	3.1416
5	SLIM Synchronous velocity V_s (m/s)	17.22	17.22	16.32	16.31
6	Rotor velocity V_r (m/s)	15.5	15.5	15.5	15.5
7	No of poles p	4	4	4	4
8	Pole pitch τ (m)	0.1435	0.1435	0.136	0.1360
9	Slot pitch λ (m)	0.0478	0.0478	0.0453	0.0453
10	Stator length L_s (m)	0.5741	0.574	0.5438	0.544
11	"Target" thrust F_s' (N)	8611	8611	8171	8171
12	Number of turns per slot N_c	7	3	5	2
13	Number of turns per phase N_l	28	12	20	8
14	Copper wire size in winding:	#5	#6	#5	#3
15	Diameter without insulation D_w (mm)	4.62	4.1148	4.62	5.826
16	Parallel wires, N_p	4	5	8	3
17	Slot width w_s (m)	0.022	.0228	0.022	.0197
18	Tooth width w_t (m)	0.0258	.0251	0.0233	.0256
19	Minimum tooth width w_{min}	-	.0069	-	.0103
20	Slot depth h_s (m)	0.0367	.0125	0.0515	.0116
21	Stator core yoke height h_y (m)	0.0075	.0162	0.01	.0242
22	Actual thrust at specified V_r, F_s (N)	7357	8610	6393	9651
23	Output power at specified V_r, P_{out} (kW)	114.04	133.45	99.1	149.6
24	Input power at specified V_r, P_{in} (kW)	134.84	161.54	112.64	176.6
25	Stator efficiency at specified V_r, η (%)	84.58	82.62	87.97	84.7
26	Actual rated stator RMS current I_l (A)	321	407.13	541	810.53
27	Actual stator current density J_l (A/mm ²)	4.79	6.12	4.03	10.13
28	Total length of copper wire T_{lw} (m)	1094	1182.06	1586	471.97
29	Total weight of copper wire W_{copper} (kg)	163	176.21	236	111.85
30	Iron core weight W_{iron} (kg)	389	326.35	491	415.7
31	Total weight of one stator unit W_{stator} (kg)	552	502.56	727	527.55

CHAPTER 6

CONCLUSIONS AND SUGGESTIONS

In this project, a detailed study of the design of the SLIM was performed and compared with that of a comparable TLIM design. The main objective of this project was to formulate the design equations of the SLIM and then develop a user-interactive computer program for its design. The equivalent circuit model of the SLIM was studied in order to obtain the performance equations for thrust and efficiency. The SLIM design algorithm is made completely user-interactive where the user has the convenience of choosing various design parameters like the primary voltage and frequency, number of poles, number of phases and many more. Also, the basic design algorithm from Plodpradista [29] is modified by including a look up table for all the wire gauges and also an extra iterative loop which will make the slot width to tooth width ratio close to 50% matching all the other design constraints.

6.1. Conclusions

It can be concluded that the air-gap plays a very important role in the performance of the SLIM. The air-gap needs to be as small as possible to have a better thrust and efficiency. Another crucial design parameter is the thickness of rotor outer layer which is aluminum. As the thickness of the aluminum sheet is increased thrust also increases along

with the length of magnetic air-gap which is undesirable. Hence, care should be taken in choosing the best value for aluminum thickness which yields maximum thrust at a reasonable efficiency. The number of poles in the stator was the last parameter that was varied to observe the SLIM performance curves. By increasing the number of poles, the end effects are reduced, which is good for the SLIM performance. At the same time thrust is increased but at the expense of efficiency. Hence, there is a trade off between the thrust and the efficiency with increasing number of poles.

So, from the parametric evaluation which is performed in Chapter 5, it can be concluded that the input parameters like the length of physical air-gap, the thickness of aluminum sheet and the number of poles play a vital role in the performance parameters, thrust and efficiency. Therefore, care should be taken in choosing these parameters. Based on our target values of rotor velocity and thrust, these parameters should be chosen which gives the best possible thrust closest to the target value at a decent value of efficiency.

Finally, the design parameters of SLIM and a similar TLIM are compared in table 5-4. It can be seen that by introducing an extra iterative loop in the design algorithm, a better performance parameters can be obtained compared to TLIM [29]. Hence it can be concluded that the design algorithm was modified appropriately to get better results for the design of the SLIM having the same design parameters as that of a TLIM shown in [29]. Also the final thrust from this design is very close to the target thrust which is desirable.

6.2. Suggestions for Future work

This study of SLIM neglected several issues like end effects and edge effects, which will affect the performance of the SLIM. There are some improvements which can be implemented in the design of SLIM for better analysis. Some suggestions for future study are as follows:

1. Improving the equivalent circuit model of the SLIM by introducing various realistic factors like end effects, edge effects, air-gap leakage fluxes and skin effects due to finite plate thickness.
2. Use the finite element method (FEM) analysis instead of equivalent circuit model for determining the SLIM performance.
3. Detailed study must be done regarding the layout of stator windings by building a laboratory model of the SLIM. Improvements to the proposed model can be suggested by trying different winding configurations.
4. The SLIM is designed and analyzed in its steady state only. The transient behavior of the SLIM is not analyzed in this study. This can be done as a future extension of this project.
5. The slip can be varied to get the thrust close to the target value from the performance curves for a particular design. This can be implemented in the future, using algorithms of curve fitting and root finding.

APPENDIX A

WIRE GAUGE TABLE FOR COPPER WIRE

AWG gauge	Diameter (mm)	Ohms per Km	Ampacity (Amps)	Ft per pound
0000	11.684	.1607	312	20400.0
000	10.4038	.2027	262	16180.0
00	9.26592	.2555	220	12830.0
0	8.25246	.3224	185	10180.0
1	7.3482	.4064	156	8070.0
2	6.543	.5126	131	6400.0
3	5.8267	.6461	110	5075.0
4	5.1892	.8151	92.3	4025.0
5	4.6202	1.0276	77.6	3192.0
6	4.1148	1.2959	65.2	2531.0
7	3.6652	1.6341	54.8	2007.0
8	3.2639	2.0605	46.1	1592.0
9	2.90576	2.5981	38.7	1262.0
10	2.58826	3.2764	32.5	1001.0
11	2.30378	4.1328	27.3	794.0
12	2.05232	5.2086	23	629.6
13	1.8288	6.5698	19.3	499.3
14	1.62814	8.282	16.2	396.0
15	1.45034	10.443	13.6	314.0
16	1.29032	13.173	11.5	249.0
17	1.15062	16.61	9.6	197.5
18	1.02362	20.943	8.1	156.6
19	.91186	26.407	8.25	124.2
20	.8128	33.292	10.12	98.5
21	.7239	41.984	12.76	78.1
22	.6451	52.939	16.25	62.0
23	.5740	66.780	20.3	49.1
24	.5105	84.197	25.6	39.0
25	.4546	106.17	32.2	30.9
26	.4038	133.85	40.7	24.5
27	.3607	168.82	51.3	19.4
28	.3200	212.87	64.8	15.4
29	.2870	268.4	81.6	12.2
30	.254	338.49	103	9.7
31	.226	426.73	130	7.7
32	.203	538.25	164	6.1

APPENDIX B

USER-INTERACTIVE COMPUTER PROGRAM (USING MATLAB)

```
% SLIM Design Using a Matlab Program
clear all;
clc;
%Assign necessary constants and parameters
mu0 = 4*pi*10^-7;
rho_w = 19.27*10^-9;
rho_r = 28.85*10^-9;
btmax = 1.6;
bymax = 1.3;
J1 = 6e6;
%Assign desired values for certain variables
d = input('Enter Aluminum thickness (in meters) = ');
m = input('Enter the number of phases = ');
Vline = input('Enter the primary line to line voltage = ');
V1 = Vline/sqrt(3);
f = input('Enter the supply frequency = ');
p = input('Enter the number of poles = ');
q1=input('Enter the number of slots per pole per phase= ');
Srated = input('Enter the rated slip = ');
Ws = input('Enter the width of the stator = ');

%Data from the PCP design procedure
Fsprime = input('Enter the target thrust = ');
Vcrated= input('Enter rated rotor velocity = ');
```

```

Vs= Vcrated/(1 - Srated);
tau = Vs/(2*f);
lambda = tau/(m*q1);
Ls = p*tau;

for i = 1:30
    N1 = p*q1*i;
    ncos0 = 0.2;
    ncos1(i) = 1;
    while abs(ncos0 - ncos1(i))>0.0001

        Ilprime = (Fsprime*Vcrated)/(m*V1*ncos0);
        Aw = Ilprime/J1;
        As = (10*i*Aw)/7;
        ws = lambda/2;
        wt = ws;
        hs = As/ws;
        gm = 0.01;
        go = gm + d;
        gamma = (4/pi)*(((ws/(2*go))*atan(ws/(2*go))) -
            log(sqrt(1 + ((ws/(2*go))^2))));
        kc = lambda/(lambda - gamma*go);
        ge = kc*go;
        kw = sin(pi/(2*m))/(q1*sin(pi/(2*m*q1)));
        G = 2*mu0*f*tau^2/(pi*(rhor/d)*ge);
        a=pi/2;
        ae=a+ge/2;
        Lce=tau;
        beta1=1;
        lamda_s= (hs*(1+3*beta1))/(12*ws);
        lamda_e= (0.3*(3*beta1-1));
    end
end

```

```

lamda_d= 5*(ge/ws)/(5+4*(go/ws));

%Equivalent Circuit Components
R1(i)=rhow*(4*a+2*Lce)*J1*N1/I1prime;
a1(i)=lamda_s*(1+3/p)+lamda_d;
b1(i)=lamda_e*Lce;
X1(i)=8*mu0*pi*f*((a1(i)*2*a/q1)+b1(i))*N1^2/p;
Xm(i)= (48*mu0*pi*f*ae*kW*N1^2*tau)/(pi^2*p*ge);
R2(i) = Xm(i)/G;

Z(i)=R1(i)+j*X1(i)+((j*R2(i)*Xm(i))/Srated)/((R2(i)/Sr
ated) + j*Xm(i));

I1(i) = V1/abs(Z(i));
I2(i) = j*I1(i)*Xm(i)/(R2(i)/Srated+j*Xm(i));
Im(i) = I1(i) - I2(i);

%Actual TLIM Thrust
Fs(i) = (m*abs(I1(i))^2*R2(i))/(((1/(Srated*G)^2)+
1)*Vs*Srated);
diff(i) = Fs(i) - Fsprime;
dmin = min(abs(diff));
Pout = Fs*Srated;
Pin=Pout+m*abs(I2(i))^2*R2(i)+m*abs(I1(i))^2*R1(i);
eta = Pout/Pin;
PF = cos(angle(Z(i)));
ncos1(i)=eta*PF;
ncos0=(ncos0+ncos1(i))/2;
end;
end;
k = 1;

```

```

while dmin~=abs(diff(k))
    k = k + 1;
end;
Nc = k;
Nl = p*q1*Nc;
Fs = Fs(k);
I1 = I1(k);
ncos1 = ncos1(k);
A=[3  5.8;4  5.189;5  4.62;6  4.1148;7  3.665;8  3.2639;9
2.9057;10 2.588 ];
guage=0;
while (guage<8)
    guage=guage+1;
    pw = 0;
    r=0;
    wt = 1;
    wtmin= 0;
    g=0;r=0;
    while (wt-wtmin)>0.0152
        r=r+1;
        g=g+1;
        wire_d=A(guage,2);
        pw = pw + 1;
        ws = (wire_d*10^-3*pw) + 2.2*10^-3;
        wt = lambda - ws;
        Aw = pw*pi/4*wire_d^2*1e-6;
        As = (10*Nc*Aw)/7;
        hs = As/ws;
        gm = 0.01;
        go = gm + d;
        gamma=(4/pi)*(((ws/(2*go))*atan(ws/(2*go)))-

```

```

log(sqrt(1 + ((ws/(2*go))^2)));
kc = lambda/(lambda - gamma*go);
ge = kc*go;
G = 2*mu0*f*tau^2/(pi*(rhor/d)*ge);
kw=sin(pi/(2*m))/(q1*sin(pi/(2*m*q1)));
a=pi/2;
ae=a+ge/2;
Lce=tau;
beta1=1;
lamda_s= (hs*(1+3*beta1))/(12*ws);
lamda_e= (0.3*(3*beta1-1));
lamda_d= 5*(ge/ws)/(5+4*(go/ws));

%Equivalent Circuit Components
R1=rhow*(4*a+2*Lce)*J1*N1/Iprime;
a1=lamda_s*(1+3/p)+lamda_d;
b1=lamda_e*Lce;
X1=8*mu0*pi*f*((a1^2*a/q1)+b1)*N1^2/p;
Xm=(48*mu0*pi*f*ae*kw*N1^2*tau)/(pi^2*p*ge);
R2 = Xm/G;
Z=R1+j*X1+(R2/Srated*j*Xm)/(R2/Srated+j*Xm);
I1 = V1/abs(Z);
I2 = j*I1*Xm/(R2/Srated+j*Xm);
Im=I1-I2;
wtmin=2*sqrt(2)*m*kw*N1*abs(Im)*mu0*lambda/(pi*p*ge*bt
max);
end;
hy=4*sqrt(2)*m*kw*N1*abs(Im)*mu0*Ls/(pi*pi*p*p*ge*bymax);
para_wires(guage)=pw;
slot_width(guage)=ws;

```

```

tooth_width(guage)=wt;
min_toothwidth(guage)=wtmin;
height_slot(guage)=hs;
Area_wire(guage)=Aw;
Area_slot(guage)=As;
Num_c(guage)=Nc;
Num_l(guage)=Nl;
Sta_I(guage)=I1;
gap_e(guage)=ge;
current_den(guage) = abs(I1)/Aw;
height_yoke(guage)=4*sqrt(2)*m*kw*N1*(Im)*mu0*Ls/(pi*pi*
i*pi*ge*bymax);
final_thrust(guage)=(m*abs(I1)^2*R2)/(((1/(Srated*G)^2
)+1)*Vs*Srated);
output(guage)=final_thrust(guage)*Vcrated;
input(guage)=output(guage)+m*abs(I2)^2*R2+m*abs(I1)^2*
R1;
efficiency(guage)= output(guage)/input(guage);
difference(guage)=final_thrust(guage)-Fsprime;
diffmin(guage) = min(abs(difference));
end;
kk = min(diffmin);
jj=1
while kk~=abs(diffmin(jj))
    jj = jj + 1;
end;
best_wireguage=A(jj,1)

$$$$ To Generate the Characteristic curves $$$

vel_sta= 17.22;

```



```

slip= 0.1;
e=1;
for slip=0.000001:0.01:1
    vel_rot(e)=vel_sta*(1-slip);
    impz(e) = R1+j*Xl+(R2/slip*j*Xm)/(R2/slip+j*Xm);
    i1(e) = V1/abs(impz(e));
    i2(e) = j*i1(e)*Xm/(R2/slip+j*Xm);
    im(e) = i1(e)-i2(e);
    Force(e)=(m*(abs(i1(e)))^2*R2)/(((1/(slip*G)^2)+1)*vel
    _sta*slip);
    out_pow(e) = Force(e)*vel_rot(e);
    in_pow(e)=out_pow(e)+m*abs(i2(e))^2*R2+m*abs(i1(e))^2*
    R1;
    eff(e) = out_pow(e)/in_pow(e);
    e=e+1;
end;
figure(1);
plot(vel_rot,Force,'green');
hold on;
hold on;
plot([15.5 15.5],[0,Fs]);
hold on;
plot([0 15.5],[Fs Fs]);
hold on;
figure(2);
plot(vel_rot,eff*100,'green');
hold on;
plot([15.5 15.5],[0 eta*100]);
hold on;
plot([0 15.5],[eta*100,eta*100]);
hold on;

```

REFERENCES

- [1] Nasar, S.A. and Boldea, I., *Linear Electric Motors*, Prentice-Hall, Inc., Englewood Cliffs, New Jersey, 1987.
- [2] “Electrical traction independent of adhesion,” *Le Genie Civil*, pp. 381-382, 1901.
- [3] Zehden, A., “Travelling wave electric traction equipment,” French patent 321 692, applied for June 2, 1902.
- [4] Zelenay, Rosenfeld, and Dulait, “Travelling wave applied to electric railways,” French patent 318 634, Feb. 12, 1902.
- [5] Rosenfeld and Zelenay, “Tangential traction,” *Bull. Ass. Ing. Mantefiore*, Vol. 3, pp. 214-238, 1903.
- [6] Birkeland, K., Norwegian Patents 11 228, Apr. 22, 1902, and 13 052, Apr. 23, 1903.
- [7] “A wound rotor, 1400 feet long,” *Westinghouse Engineer*, pp. 160-161, Sept. 1946.
- [8] Jones, M.F., “Three phase linear motor catapult system,” U.S.Patent 2 404 984, July 30, 1946.
- [9] Hermant, C., “Improvements to the linear induction electromagnetic pumps,” *Bull. Soc. Fr. Elec.*, pp. 163-178, 1960.
- [10] Laithwaite, E.R., *Induction machines for special purposes*, Chemical publishing Company, Inc., new York, 1966.
- [11] Yamamura, S., *Theory of Linear Induction Motors*, 2nd Edition, John Wiley & Sons, Inc., New York, 1979.
- [12] Poloujadoff, M., *The theory of Linear Induction Machinery*, Oxford University Press, Inc., New York, 1980.
- [13] Boldea, I. and Nasar, S.A., *Linear Motion Electromagnetic systems*, John Wiley

- & Sons, Inc., New York, 1985.
- [14] Gieras, J.F., *Linear Induction Drives*, Oxford University Press, Inc., New York 1994.
- [15] A complete equivalent circuit of a linear induction motor with sheet secondary
Pai, R.M.; Boldea, I.; Nasar, S.A.; Magnetics, IEEE Transactions on , Volume: 24 , Issue: 1 , Jan. 1988 Pages:639 – 654.
- [16] The causes and consequences of phase unbalance in single-sided linear induction motors
Adamiak, K.; Ananthasivam, K.; Dawson, G.E.; Eastham, A.R.; Gieras, J.F.; Magnetics, IEEE Transactions on , Volume: 24 , Issue: 6 , Nov 1988 Pages:3223 – 3233.
- [17] LIM dynamic performance assessment from parameter identification
Zhang, Z.; Eastham, T.R.; Dawson, G.E.; Industry Applications Society Annual Meeting, 1993., Conference Record of the 1993 IEEE , 2-8 Oct. 1993 Pages:295 - 300 vol.1.
- [18] Adapting a linear induction motor for the acceleration of large masses to high velocities
Laithwaite, E.R.; Electric Power Applications, IEE Proceedings-, Volume: 142 , Issue: 4 , July 1995 Pages:262 – 268.
- [19] The thrust and the Relation Factor k_r in linear induction machines
Simone, G.A.; Creppe, R.C.; de Souza, C.; Electric Machines and Drives Conference Record, 1997, IEEE International , 18-21 May 1997 Pages:MB1/11.1 - MB1/11.3.
- [20] Characteristics of two-phase levitated linear induction motor,
Tachino, K.; Amei, K.; Maeda, T.; Sakui, M.; Power Electronics and Drive Systems, 1999. PEDS '99. Proceedings of the IEEE 1999 International Conference on, Volume: 1, 27-29 July 1999 Pages: 281 - 285 Vol.1.
- [21] Accurate modelling of single-sided linear induction motor,
Faiz, J.; Jafari, H.; Magnetics Conference, 1999. Digest of INTERMAG 99. 1999 IEEE International, May 18-21, 1999 Pages: AS19 - AS19.
- [22] Obtaining the operating characteristics of linear induction motors: a new approach
Mirsalim, M.; Doroudi, A.; Moghani, J.S.; Magnetics, IEEE Transactions on, Volume: 38, Issue: 2, March 2002 Pages: 1365 – 1370.
- [23] Aboudara, D.N., et al., “Tomorrow’s mass rapid transit available today,” *IEEE Spectrum*, vol. 4, pp. 61-70, Jan.1967.
- [24] Kawakami, T., “Electrical features of the New Tokaido Line,” *IEEE Spectrum*, vol. 3, pp 57-63, Jan. 1966.

- [25] Poloujadoff, M., Linear induction machines, Part II – Applications, *IEEE Spectrum*, March 1971, pp. 77-86.
- [26] “Feasibility of using Pneumatic capsule pipelines in New York City for Underground Freight Transport”, Dr. Henry Liu, paper for presentation at *ASCE pipeline Conference*, San Diego, California, Aug. 1-4, 2004.
- [27] Del Toro, V., *Electric Machines and Power Systems*, Prentice-Hall, Inc., Englewood Cliffs, New Jersey, 1985.
- [28] Assadollahbaik, M., Linear Induction motor for pumping capsules in pipes, Ph.D. Dissertation, Department of Civil Engineering, University of Missouri- Columbia, July 1984.
- [29] Wisuwat Plodpradistha, Study of Tubular Linear Induction Motor for Pneumatic Capsule Pipeline system, Ph.D. Dissertation, Department of Electrical Engineering, University of Missouri- Columbia, May 2002.
- [30] S.A.Nasar and I.Boldea, *Linear motion Electric Machines*, John Wiley and Sons., New York 1976.
- [31] Still, A. and Sisikind, C.S., *Elements of Electrical Machine Design*, McGraw-Hill Book Company, Inc., New York, 1954.
- [32] Sarma, M.s., *Electric Machines – Steady-State Theory and Dynamic Performance*, WM.C.Brown Publishers. Dubuque, Iowa, 1985.
- [33] Stephen J. Chapman, *Electric Machinery Fundamentals*, McGraw-Hill, 1999.
- [34] Viet Nam Hoang, “Design of Single-Sided Linear Induction Motor”, Bachelor of Electrical Engineering Project, School of Information Technology and Electrical Engineering, University of Queensland, 2003.
- [35] M.G.Say, *Theory of Alternating current Machines*, John Wiley & Sons Publications.